Landslides (2021) 18:2785–2812
DOI 10.1007/s10346-021-01661-1
Received: 22 September 2020
Accepted: 26 March 2021
Published online: 4 May 2021

Costanza Morino · Susan J. Conway · Matthew R. Balme · Jón Kristinn Helgason · Þorsteinn Sæmundsson · Colm Jordan · John Hillier · Tom Argles

The impact of ground-ice thaw on landslide geomorphology and dynamics: two case studies in northern Iceland

Abstract As consequence of ongoing climate change, permafrost degradation is thought to be increasingly affecting slope stability in periglacial environments. This is of growing concern in Iceland, where in the last decade, permafrost degradation has been identified among the triggering factors of landslides. The role of ground ice in conditioning the morphology and dynamics of landslides involving loose deposits is poorly understood. We show the geomorphological impact of the Móafellshyrna and Árnesfjall landslides that recently occurred in ice-cemented talus deposits in northern Iceland. Using field and aerial remote-sensing measurements of the morphological and morphometric characteristics of the landslides, we assess the influence of thawing ground ice on their propagation style and dynamics. The two mass movements are complex and are similar to rock- and debris-ice avalanches, changing trajectory and exhibiting evidence of transitioning their style of motion from a dry granular mass to a debris flow-like movement via multiple pulses. We infer that the thawing of ground ice together with the entrainment of saturated material provided the extra fluid causing this change in dynamics. The hazardous consequences of permafrost degradation will increasingly affect mountain regions in the future, and ground-ice thaw in steep terrain is a particularly hazardous phenomenon, as it may induce unexpected long-runout failures and can cause slope instability to continue even after the landslide event. Our study expands our knowledge of how landslides develop in unstable ice-cemented deposits and will aid assessment and mitigation of the hazard that they pose in Iceland and other mountainous periglacial areas.

Keywords Landslides · Permafrost · Ground ice · Iceland · Risk

Introduction and state of the art

Rapid mass movements are one of the most obvious reactions to climate change of mountain slopes affected by permafrost (e.g. Fischer et al. 2006; Allen et al. 2011; Huggel et al. 2012; Haeberli et al. 2017; Patton et al. 2019). The influence of the changing cryosphere on the stability of rock walls is well documented (e.g. Gruber and Haeberli 2007; Krautblatter et al. 2013; Draebing et al. 2014; Magnin et al. 2017; Ravanel et al. 2017), while the frequency of periglacial rock falls has increased over the past century in cold mountain environments worldwide (e.g. Haeberli et al. 2011; Clague et al. 2012; Kellerer-Pirklbauer et al. 2012; Phillips et al. 2017; Beniston et al. 2018). Active layer detachments and thaw slumps caused by permafrost degradation are also well documented in areas with continuous and discontinuous permafrost (Huscroft et al. 2004; Lewkowicz and Harris 2005; Lacelle et al. 2010; Ashastina et al. 2017).

Few examples of rapid mass movements involving loose deposits, such as debris flows and debris slides, in ground-ice cemented terrains are reported in the literature (Huscroft et al. 2004; Brideau et al. 2009; Lyle et al. 2014; Sæmundsson et al. 2018), and little is known about how their dynamics are conditioned by thawing ground ice. Direct observation during or immediately after the occurrence of rapid mass movements involving frozen debris, such as talus or moraine deposits, is rare. This is because, once mobilised, frozen material thaws rapidly; furthermore, this type of landslide commonly occurs in remote glacial and periglacial areas, so they are either not observed or reported a long time after their occurrence when direct evidence of the presence of ice has gone. Nevertheless, these sparse observations help to understand the effect of ice on the mobility of the landslide. For example, at the Little Salmon Lake landslide, a debris slide in Yukon, debris cemented by ground ice was observed in the deposits a few days after the occurrence of the failure (Lyle et al. 2004, 2014). At this location, ground ice is thought to have provided cohesion to blocks of surficial material that were then "mobilized by high pore water pressure in the surrounding saturated sediments", and ground ice degradation is inferred to have caused the failure (Brideau et al. 2009).

In this paper, we aim to describe and discuss how the presence of ground ice has affected the morphology and behaviour of the Móafellshyrna and Árnesfjall landslides in Iceland (Fig. 1). Specifically, we compare and contrast the geomorphology and dynamics of the two landslides. Sæmundsson et al. (2018) estimated from visual inspection a volume percentage of 15–20% ground ice of the material mobilised by both landslides. We assess how this relatively low ice content has affected the mechanical behaviour of the debris compared to rock/debris slides/avalanches. We show field evidence and describe and quantify the morphometric characteristics of these two landslides and determine how the thawing of ground ice has affected their emplacement. This study contributes to the understanding of a complex type of landslide, as we show how ground ice has an impact on landslide morphology and dynamics and should be included when evaluating the potential hazard posed by rapid mass movements in periglacial areas.

Settings of the case studies

The Móafellshyrna Mountain, Tröllaskagi peninsula

The first case study is the Móafellshyrna landslide. The site is in the Tröllaskagi peninsula in northern Iceland, a mountain plateau with summits up to 1550 m high (Fig. 2a, b). The occurrence of the Móafellshyrna landslide was first witnessed by the Þrasastaðir farm residents (Sæmundsson et al. 2018), situated on the northern side of the Fljótaá river, facing the Móafellshyrna ridge (Fig. 2c).

Fig. 1 Blocks and ridges of ice-cemented sediments. **a** An oblique view of the Móafellshyrna landslide on the day of its occurrence, with one of the blocks of ice-rich sediments found in its deposits (see circles). **b** A close-up photo of the block of ice-rich sediments shown in Fig. 1a, taken 9 days after the occurrence of the Móafellshyrna landslide (in the circles, a close-up image of the ground ice cementing the deposits with a walking pole for scale). **c** One of the ridges of ice-cemented deposits found 2 days after the Árnesfjall failure. **d** Ground ice found at 1 m of depth in the landslide deposits 2 days after the occurrence of the Árnesfjall landslide

The bedrock of the mountain is within the Tertiary basalt series and consists of closely jointed basaltic layers, interbedded with poorly cohesive red to yellow hyaloclastites, with thicknesses from a few centimetres up to decametres. Horizons of red lithified paleosols up to few metres thick are also observable in the basaltic sequence. The 15 to 10 Ma old basaltic layers (Jóhannesson 2014) dip 5–10° towards SW-WSW on average and are cut by 3 and 7 Ma old dikes, sills and faults (Garcia et al. 2003).

The landscape of the whole Tröllaskagi peninsula has been sculpted by the Icelandic Ice sheet, which abruptly retreated at the end of the Preboreal period (e.g. Andrews et al. 2000; Geirsdóttir et al. 2009; Pétursson et al. 2015; Andrés et al. 2019), and is characterised by deeply incised glacial valleys and cirques. A total of 167 glaciers, mostly debris-covered, are catalogued on the peninsula, all in regions above 800 m a.s.l. (Andrés et al. 2016). Perennial snow patches (Tussetschläger et al. 2020), active rock glaciers and stable ice-cored moraines are abundant in the region (Farbrot et al. 2007a; Lilleøren et al. 2013), with the latter two being used to calibrate numerical models of mountain permafrost (Farbrot et al. 2007b; Etzelmüller et al. 2007). The lower mountain permafrost limits in Tröllaskagi have been modelled at 600–900 m a.s.l. at windy sites and at 1000–1150 m a.s.l. in snow-rich areas (Etzelmüller et al. 2007; Czekirda et al. 2019). According to the model output, the warming trend of the last three-four decades in Iceland has led to permafrost degradation. This is also testified by the presence of molards—cones of loose debris derived from the thawing of blocks of ice-rich sediments mobilised by landslides in permafrost terrains—that have been found in the deposits of the two landslides analysed in this paper and that are considered to be an indicator of permafrost degradation (Milana 2016; Morino et al. 2019).

The Móafellshyrna landslide originated at 873 m a.s.l. and travelled 1320 m on the north-west facing slope of the mountain. The topographic long profile of the landslide can be subdivided into five distinct sections (Fig. 3):

- Section 1 is the detachment zone. It includes the headscarp, the topographic bench from which the source deposits detached, and the bedrock cliff over which the mass fell. The highest elevation of the headscarp is 873 m a.s.l., and its elevational extent is 183 m. This section has a staircase-shaped profile: the headscarp has an average slope of 36°; then, there is a break-in slope leading to the bench, which has an average slope of 14°, and then further downslope the cliff has a slope of 44°;
- Section 2 is the first transport zone. It consists of the talus slope below the topographic bench, with an average slope of 31°. The top of this section is at 690 m a.s.l., and the elevation drop is 180 m;
- Section 3 is the first low slope (16°) accumulation zone, and its top is at 510 m a.s.l. with an elevation drop of 30 m;
- Section 4 is the second transport zone. The topographic profile has a convex-up shape, with its top located at 480 m a.s.l, an elevation drop of 90 m, and an average slope of 23°;
- Section 5 is the second accumulation zone. Its top is at 390 m a.s.l., and it has an average slope of 14°. The landslide toe is located at 329 m a.s.l.

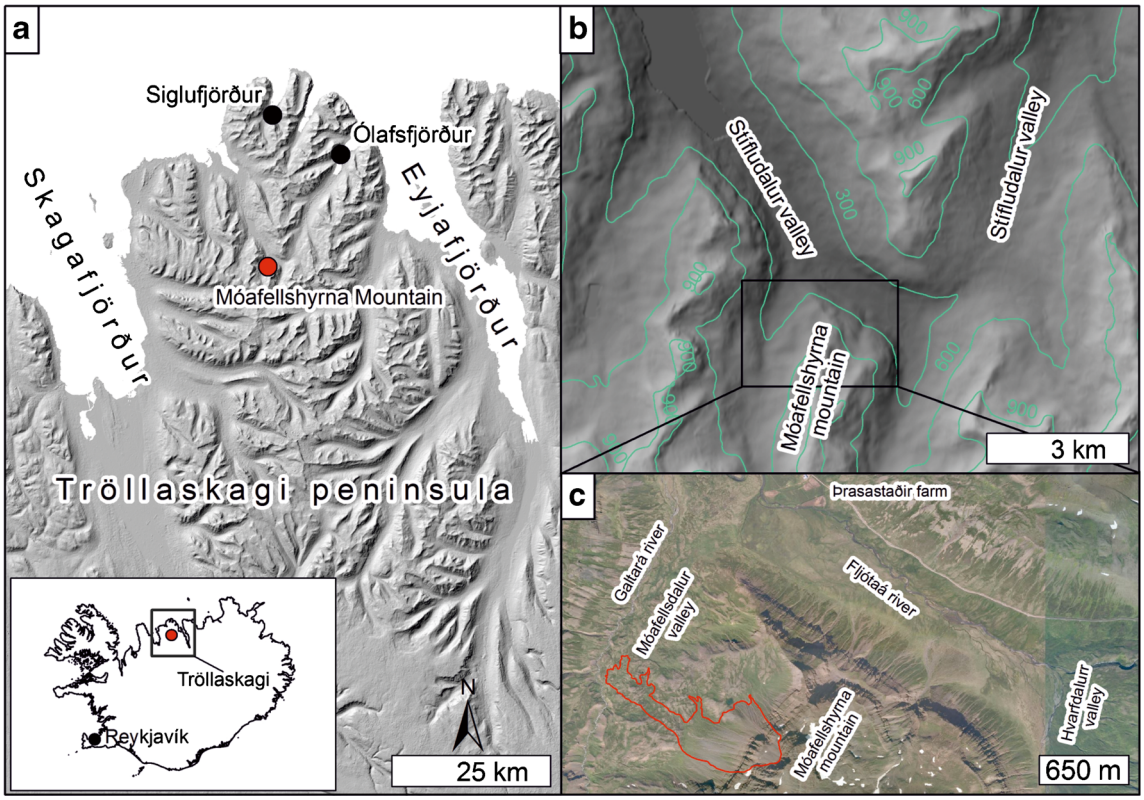

Fig. 2 The geographic setting of the Móafellshyrna site, Tröllaskagi peninsula, northern Iceland. **a** A hillshaded digital elevation model (DEM) showing the main geographic locations of Tröllaskagi peninsula and the Móafellshyrna Mountain (DEM source EU-DEM from the Global Monitoring for Environment and Security service for geospatial reference data access project (GMES RDA). **b** Hillshaded DEM and contours (in green, m above sea level) of the Móafellshyrna region. **c** Aerial photograph (source samsyn.is) of the Móafellshyrna Mountain before the landslide (perimeter of the landslide marked by a red line) in 2012, showing some of the main geographic features of the area

This step-like topographic profile is not caused by the morphological changes produced by the failure, but follows the underlying topography, typical of periglacial landscapes that have undergone recent deglaciation. This kind of profile is known as the "free-face model" and is composed of a rockwall above 40° below which there is, first, a talus slope, and then, second, a footslope or a basal complex (King 1953; French 2007).

The Árnesfjall Mountain, Westfjords

The second case study is the Árnesfjall landslide, located on the coast and 26 km ESE of the southern terminus of the Drangajökull glacier (Fig. 4a). The Árnesfjall Mountain rises from sea level to 490 m of elevation (Fig. 4b).

The bedrock of the mountain is within the Tertiary basalt series and consists of superimposed basaltic lava flows (Miocene–Lower Pliocene; Jóhannesson 2014). Individual lava layers are sub-horizontal (locally dipping 5–10° towards ESE), 2 to 30–40 m thick, and are interlayered by red lithified paleosols, a few centimetres to a few metres thick, and sometimes volcaniclastic sedimentary horizons. Intrusions of rhyolite crop out on the northern slope of the mountain. The Westfjords are characterised by deep fjords, glacial valleys and wide cirques, while the mountains have extensive flat summits (up to 998 m a.s.l.) and steep flank slopes (25–35°) (Decaulne et al. 2005). The Drangajökull is the only ice cap present in the Westfjords.

The elevation of permafrost in this region could be significantly lower than the one predicted over c. 800 m a.s.l. by numerical models for the northern and central region of the island (Farbrot et al. 2007b; Etzelmüller et al. 2007), because of lower summer temperatures, shorter melting season, frequent northerly polar winds and the proximity at less than 25 km of the Drangajökull ice cap, around which the presence of permafrost has been hypothesised (Glade 2005; Brynjólfsson et al. 2014). As in the Móafellshyrna case, molards have been found in the Árnesfjall landslide's deposits and interpreted as marker of permafrost degradation (Morino et al. 2019).

The Árnesfjall landslide originated at 420 m a.s.l. from the north facing slope of Árnestindur and travelled 563 m. The topographic long profile of the landslide can be subdivided into three sections (Fig. 5):

- Section 1 is the detachment zone, which consists of the headscarp and the bedrock exposed from underneath the landslide mass. The top is located at 418 m a.s.l., the elevation drop is 60 m, and the section has an average slope of 37°;

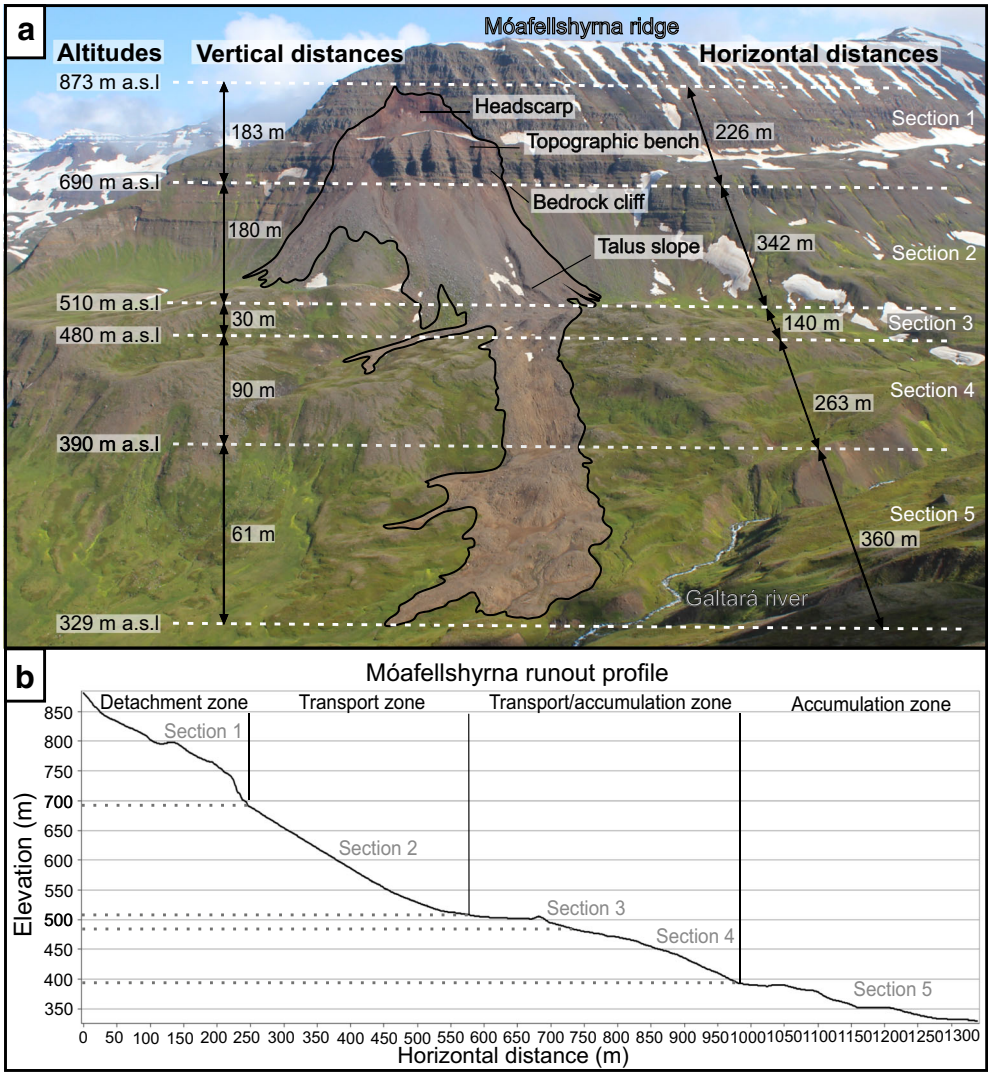

Fig. 3 The division of the Móafellshyrna landslide into sections based on topography and whether erosion, transport or accumulation dominates. **a** Oblique view, looking south-east, of the Móafellshyrna landslide with the different sections outlined. **b** Longitudinal topographic profile divided into five sections, corresponding to the detachment, transport, transport/accumulation and accumulation zones detailed in the text and marked in **a**

- Section 2 is the depletion zone (as defined by Cruden and Varnes (1996), namely the area of the landslide where the displaced mass overlies the rupture surface and underlies the original ground surface), with the top at 358 m a.s.l., an elevation drop of 42 m, and an average slope of 23°;
- Section 3 is the accumulation zone, with the top at 316 m a.s.l., an elevation drop of 246 m, and an average slope of 32°.

Weather conditions in the study areas

Iceland is characterised by frequent and sudden changes in precipitation and temperature, because the island is positioned on the main path taken by North Atlantic low-pressure systems (Einarsson 1984), and weather conditions vary among its different regions. In the Tröllaskagi peninsula, the mean annual air temperature (MAAT) for the period 1971–2000 was 2–3 °C (Tveito et al. 2000; Crochet et al. 2007; Crochet and Jóhannesson 2011). The data series between 1940 and 1970 show MAAT of 2–4 °C in the coastal areas and − 2 to − 4 °C at the mountain summits (Einarsson 1984). The Tröllaskagi peninsula is generally a snow-prone area during the winter months (Arnalds et al. 2001), and the annual precipitation from 1971–2000 varies from 1000 to 1500 mm in the coastal lowlands up to 2000–2500 mm on the mountain areas (Crochet et al. 2007).

In the Westfjords, the MAAT for the period 1961–1990 is 3.2° (Glade and Jensen, 2004), and the decadal anomaly recorded for the periods 1991–2000 and 2001–2010 with respect to the reference period 1961–1990 is, respectively, − 0.25 to 1.25 °C and 1–1.25 °C (Crochet et al. 2007). For the same period (1961–1990), in Kvígindisdalur, a station on the south side of the Westfjords that has continuous data, the mean annual precipitation was 1380 mm (Glade and Jensen 2004), while for the period 1949–1992, it was 770 mm at the station of Gjögri, in the western side of the

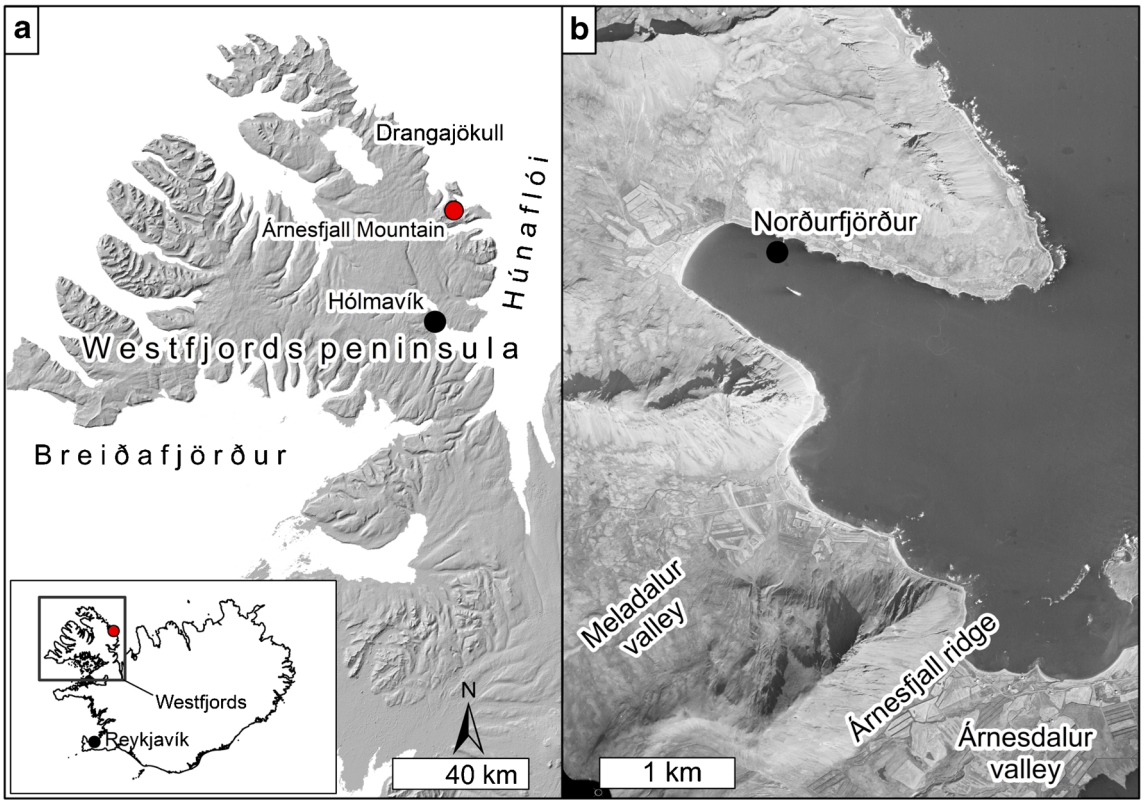

Fig. 4 The geographic setting of the Árnesfjall site, on the Westfjords peninsula, north-western Iceland. **a** The hillshaded DEM showing the main geographic locations of the Westfjords peninsula and the Árnesfjall Mountain (base map from the EU-DEM from the Global Monitoring for Environment and Security service for geospatial reference data access project (GMES RDA)). **b** Aerial photograph from 1981 (source National Land Survey of Iceland–Landmælingar Íslands) of the Árnesfjall Mountain, showing some of the main geographic features of the area

Westfjords. Average annual precipitation of 969 mm was calculated compiling data from the stations of Lambavatn, Galtarviti, Hornstrandir and Aedey in the Westfjords (Decaulne 2001). In the Westfjords, the strongest winds are most often north-easterly and bring abundant precipitation (Jónsson et al. 2004).

Methods

Fieldwork

We visited the Móafellshyrna site a few hours and subsequently 9 days after the event. We performed fieldwork at the Móafellshyrna landslide in summer 2015, 3 years after the landslide occurred. We visited Árnesfjall site 2 days after the landslide event, and we performed fieldwork in summer 2016, 2 years after the landslide occurred.

Detailed fieldwork was conducted with the purpose of identifying, characterising and classifying geomorphic features and structures of the landslides, in order to reconstruct the failure history, and to compare field observations with remote sensing datasets. We performed geological and geomorphological field analyses in every section of each landslide (see "The Móafellshyrna Mountain, Tröllaskagi peninsula" and "The Árnesfjall Mountain, Westfjords"), observing and measuring the thickness (using a measuring tape), composition and texture (using comparative charts) of the deposits. At both field sites, we performed differential GPS (dGPS) surveys of the landslides using two GNSS Leica System 1200 in Móafellshyrna and two GNSS Leica VIVA GS10 Systems in Árnesfjall (one as rover unit and one as base station; average accuracy of samples is around 1 cm in the horizontal and 2 cm in height). In Móafellshyrna, a base GPS unit was positioned on the landslide deposits, always within 1 km of the rover GPS unit, whose antenna was attached to a helmet worn by the operator. These GPS measurements were collected to survey the landslide perimeter, the thickness of the deposits and the main geomorphic features of the landslide, recording a sample every 10–15 m for at least 5 epochs (seconds) per sample. In Árnesfjall, a base GPS unit was positioned at the foot of the northern slope of the Árnesfjall mountain, within 500 m of the rover GPS unit, whose antenna was positioned on a pole. The dGPS measurements were used to survey the perimeter of the landslide, logging data when the rover was static and moving, with a record rate every 1 s. Samples were recorded every 20–30 m, recording for at least 10 epochs every sample. To ensure high quality, at both field sites, data were not collected when the Global Dilution of Precision (GDOP) value (which is calculated real-time from relative satellite positions) was > 7. Finally, dGPS units were also used to support structure from motion (SfM) data collection (see "Structure from motion").

Airborne data

In September 2015, the U.K. Natural Environment Research Council's Airborne Research Facility (NERC-ARF), on behalf of the

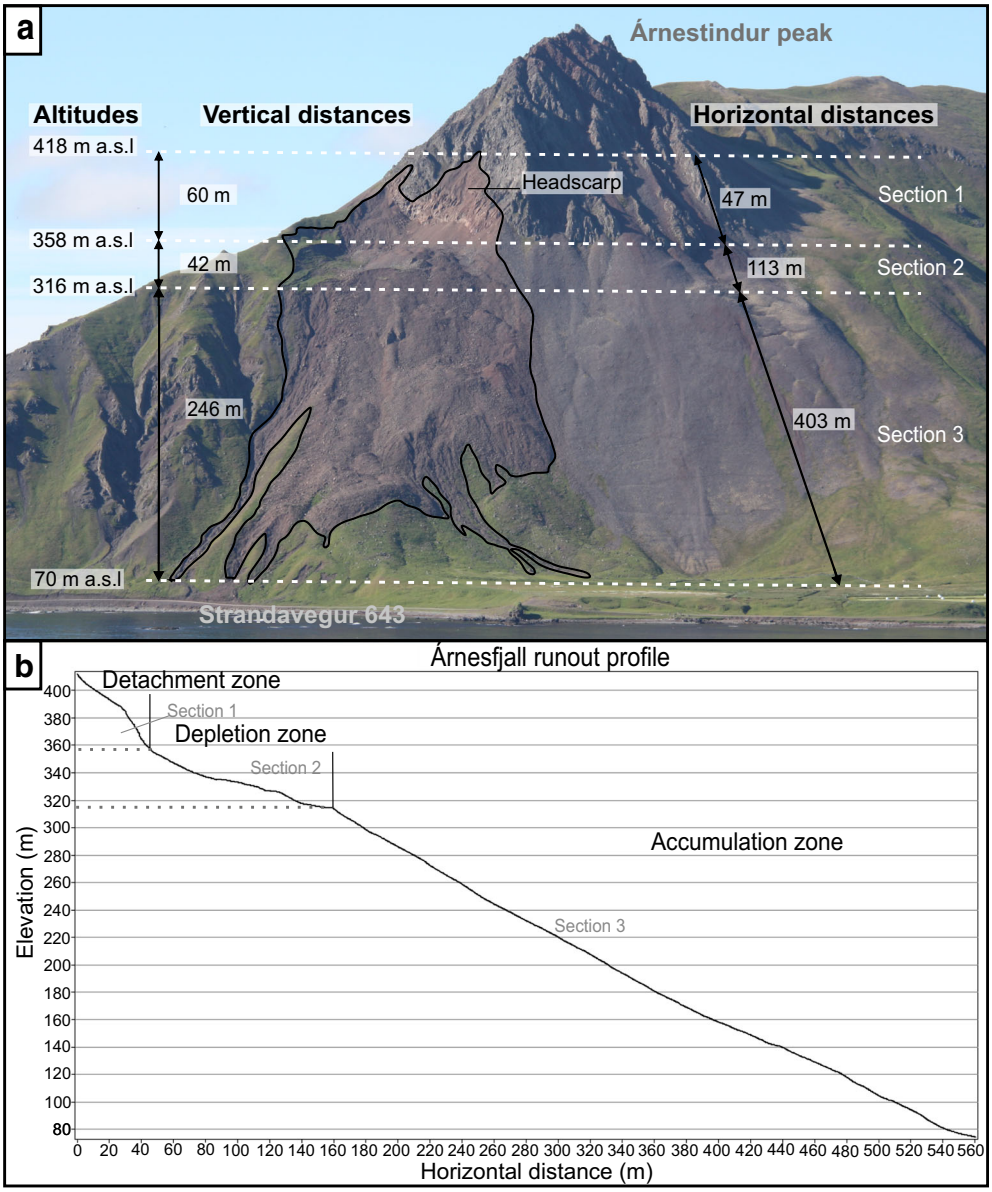

Fig. 5 The Árnesfjall landslide divided into sections based on topography and dominant process. **a** Oblique view looking south towards the Árnesfjall landslide showing its local geographic setting. **b** Topographic long profile divided into three sections, corresponding to the detachment, depletion and accumulation zones

European Facility for Airborne Research (EUFAR), collected aerial photography and airborne light detection and ranging (LiDAR) data for the Móafellshyrna area in Iceland, 3 years after the Móafellshyrna landslide occurred. A total of 170 aerial photographs were collected with a Leica RCD105 digital camera, and 15 lines were flown to collect 126 million LiDAR points with (a mean of 1.7 points/m^2) using a Leica ALS50-II instrument. The processing of the LiDAR point cloud was performed by NERC-ARF-DAN (Data Analysis Node). We used the LAStools extension for ArcGIS to convert the point clouds into gridded data at 1 m/pixel, using the return time of the last peak of light to reach the receiver from the LiDAR laser shot, which is usually assumed to be the ground return. We used Agisoft Photoscan Professional 1.3.5 software to produce a seamless orthomosaic from the air photos, where the position of the images was controlled using ten well-spread ground control points, derived by locating matching positions in a hillshaded version of the LiDAR Digital Elevation Model and the aerial photographs.

Aerial photographs of the Móafellshyrna area from August 1985 and of the Árnesfjall area from August 1981, both collected at 5486 m of elevation (provided by the National Land Survey of Iceland), were also used to analyse the pre-failure morphology of the mountain, in order to compare the source area before and after the failure and to improve the estimate of the volume of debris mobilised.

Structure from motion

For this study, to produce a base map for geomorphic mapping and analysis for the Árnesfjall site, we processed digital photos with the SfM photogrammetry technique (Westoby et al. 2012;

Micheletti et al. 2015a). The SfM technique uses a series of input images with overlapping view perspectives to simultaneously reconstruct three-dimensional (3D) camera pose and sparse scene geometry using an iterative bundle-adjustment procedure (Snavely et al. 2008; Westoby et al. 2012; Fonstad et al. 2013; James and Robson 2014; Micheletti et al. 2015a). A point cloud is then produced, increasing the density by two orders of magnitude using the estimated camera positions and image clustering, and multi-view stereo methods (e.g. Furukawa and Ponce 2010). The quality of digital elevation models (DEMs) produced using the SfM technique can be comparable to models derived from aerial or terrestrial LiDAR data (James and Robson 2012; Westoby et al. 2012; Fonstad et al. 2013; Remondino et al. 2014; Micheletti et al. 2015b; Smith et al. 2015). However, the construction of the DEM and orthomosaic using SfM is an automated workflow, in which errors can be difficult to quantify (Fonstad et al. 2013; James and Robson 2014; Remondino et al. 2014; Micheletti et al. 2015b).

We collected photographs in July 2016, 2 years after the Árnesfjall landslide occurred. The photographs were taken from ground-based oblique perspective (at approximately 3 km from the landslide), using a single-lens reflex (SLR) camera (Canon EOS 450D, 12.2-megapixel image sensor) set to a fixed focal length of 200 mm and automatic exposure settings enabled. We identified clearly visible blocks and features on the landslide—a total of 19 ground control points (GCPs)—and obtained their coordinates by using differential GPS measurements, whose errors are detailed in Table 1. Photographs were inspected manually, blurry images were deleted, and the sky was masked out of each image manually. The photographs were imported into Agisoft Photoscan Professional 1.4.1, which uses an algorithm based on the Scale Invariant Feature Transform (SIFT) object recognition system (Lowe 2004; Lindeberg 2012) to identify key points for photograph alignment. We removed any misaligned photographs at this stage and then identified the GCPs recorded in the field in the image set, importing their GPS coordinates, in order to apply an absolute coordinate system to the 3D model. Scaling and georeferencing the point cloud was achieved by applying a linear similarity transformation, which was then optimised by adjusting the camera parameters and the 3D points in order to minimise the sum of the reprojection error and the georeferencing error (Javernick et al. 2014). For the 19 ground reference points, we obtained a horizontal positional accuracy ranging from 0.05 to 0.08 m, and a vertical uncertainty ranging from 0.05 to 0.15 m. This processing procedure allowed the creation of a 3D topographic model, from which we derived an orthomosaic at 9 cm/pixel and DEM at 18 cm/pixel. The 3D model has reconstruction errors of 0.9–1.8 pixels and an absolute precision of 0.5–1.5 m. We then imported the DEM and the orthomosaic into ArcGIS for further analysis.

Finally, we have employed the same procedure using Agisoft Photoscan Professional 1.4.1 to produce a DEM at 2 m/pixel and an orthomosaic at 65 cm/pixel of the Móafellshyrna area from aerial images taken in 1985, flight line Ármannsfell- Ármannshyrna, provided by the National Land Survey of Iceland–Landmælingar Íslands. These datasets were used to make before/after-event visual comparisons, and to constrain the volume analysis described in the "Volume analysis".

Volume analysis

In order to quantify the material deposited and eroded by the landslides, we calculated the volume of debris that both landslides mobilised. Firstly, we made an estimation of the entire volume mobilised by the landslides and the volumes eroded or deposited by their different features by multiplying the estimated thickness of the deposit/depth of the erosional scar (obtained by field and dGPS measurements) for the area that they cover. These measurements are compared to those obtained using the 3D topographic data. We calculated the volumes following Conway and Balme (2014) and Coquin et al. (2019), reconstructing the pre-failure surface and deriving the deposited or eroded volumes by subtracting the pre-failure surface from the landslide surface. We defined the pre-failure surface by different means: (i) field observations and tape measurements, (ii) dGPS measurements of the perimeter of the landslides and its features and (iii) visual comparison with the pre-failure aerial photographs. We used topographic contour lines outside the area affected by the landslides as a reference to manually draw the estimated topographic contours of the pre-failure topography. This task was possible because both landslides' features have well-defined edges; in the case of Árnesfjall, the talus slope next to the landslide serves this purpose particularly well, as its surface is smooth and homogeneous, and the edges of the source area are well-defined. The topographic contour intervals used to reconstruct the pre-failure surface for the landslides and their features are reported in Table 2.

We used the reconstructed topographic contours and the topography adjacent to the landslides—or their surface features—as input data for a natural neighbour interpolation to estimate the pre-failure surface. For Móafellshyrna, we used a fixed 38° slope to reconstruct the talus slope as estimated from the pre-event DEM and neighbouring talus slopes. This allowed us to obtain a new DEM with the same resolution as the original DEM. We then calculated the difference between the original DEM and the pre-failure surface in order to obtain the volume of material transported, eroded or deposited by the landslides. Error propagation calculations by Conway and Balme (2014) suggest that such volume estimates are accurate to within 25%.

We also identified and measured the volumes of boulders that fell during the Móafellshyrna event. To distinguish them from

Table 1 Summary of estimated measurement and processing error generated during GPS data collection and processing

	Vertical error (m)	Horizontal error (m)
Instrument error	0.02	0.01
Human error	0.05	0.05
Oscillation of antenna	0.1	0.1
Error in identifying the GCP in processing phase	0.5	0.5

Table 2 Summary of the topographic contour values used to reconstruct the pre-failure surfaces of the landslides

Móafellshyrna landslide and features	Topographic contour interval	Unit
Source mass	5	m
Entrained talus deposits	2	m
Árnesfjall landslide and features	**Topographic contour value**	**Unit**
Landslide	10	m
Source mass	5	m

earlier rock falls, we used blocks with freshly broken surfaces and checked their presence in the photos taken just after the event. We have chosen only blocks that fell within the landslide perimeter, or at a few metres distance from the boundary. Whenever field measurements were not recorded, we selected boulders lying on top of the landslide deposits and measured their surface area from the aerial photographs, assuming a cubic shape to calculate their volume.

Fahrböschung

A widely recognised method to quantify the mobility of a landslide is to calculate the Fahrböschung. Fahrböschung is the mobility index of a landslide and is defined as the ratio H/L, where H is the fall height and L is the horizontal length of the landslide (Shreve 1968; Scheidegger 1973; Abele 1974). This ratio corresponds to the arctangent of the dip of the line connecting the source area to the distal fallen boulder of a rock fall or to the tip of a rock/debris slide/avalanche. This angle of dip is also known as the "Fahrböschung" angle (Heim 1932), travel angle (Cruden and Varnes 1996), reach angle (Corominas 1996) and travel distance angle (Hunter and Fell 2003). The Fahrböschung is adopted for different types of landslides, including rock and debris avalanches (Scheidegger 1973; Hsu 1975; Erismann and Abele 2001), rock falls (Corominas 1996; Copons et al. 2009) and debris flows (Iverson 1997; Rickenmann 1999). The longer the travel distance is for any given distance, the lower the value of the reach angle. Also, the ratio H/L is thought to vary inversely with the source volume (e.g. Hungr 1990; Legros 2002). For rock falls, the tangent of the reach angle is considered equivalent to the coefficient of friction of the ground surface where the rock fall starts (Shreve 1968; Scheidegger 1973). Therefore, we adopted this method for analysing the mobility of both Móafellshyrna and Árnesfjall landslides and the rock/debris fall activity associated with the Móafellshyrna landslide.

In the analysis of the Fahrböschung of the Móafellshyrna bedrock and ice-cemented debris boulders, the exact source point was not identifiable, although we assumed they originated from the edge of the continuous topographic bench (Fig. 3a), where remnants of source material are still perched. Using the final position of the fallen boulders as a reference, we constructed a "centreline" path, connecting the boulder to the nearest point where this line connects to the edge of the bench. The length of the centreline path was used as the horizontal travel distance L in the Fahrböschung calculation. We calculated the fall height H subtracting the elevations of the two points connected by the centreline. We also evaluated the Fahrböschung using 10–20 other possible lines connecting the bench with each boulder, spaced every 10 m along the edge of the bench and used their median length as the length for the horizontal travel distance L. The fall height H was obtained in the same way as for the centreline. The deviation between the Fahrböschung value calculated using the length of the centreline path from the one using the median of the other potential fall lines was below 5%. Therefore, in our results, we show the Fahrböschung calculated using the centreline of the path as the horizontal travel distance.

Meteorological data

Weather conditions antecedent to the Móafellshyrna landslides are described and discussed in detail in Sæmundsson et al. (2018), so in this paper, we will only summarise the key points of the results on precipitation and temperature data analyses. We adopted the same approach used in Sæmundsson et al. (2018), using precipitation and temperature from the weather stations operated by the Icelandic Road and Coastal Administration of Siglufjörður (WMO (World Meteorological Organization) ID: 4157) at 6 m a.s.l. (25 km north of the site) and of Ólafsfjörður (WMO ID: 4155) at 5 m a.s.l. (21 km northeast of the site) and of Öxnadalsheiði highlands pass (WMO ID: 4859) at 540 m a.s.l. (40 km south of the site; only temperature). We applied an environmental lapse rate of 0.649 °C per 100 m (Sheridan et al. 2010) to the mean temperatures recorded at all three stations as an estimate of the temperature at the source zone of the Móafellshyrna landslide.

At Árnesfjall site, at the time of the failure, the closest weather station to the landslide was the manned synoptic station of Litla-Ávík (WMO ID: 4031), operated by the Icelandic Road and Coastal Administration. The station is located along the coast at 15 m a.s.l., 5 km east to the Árnesfjall landslide and 7 km south-east to the village of Norðurfjörður. Unfortunately, there is no other weather station located within 40 km of the Árnesfjall mountain recording precipitation and/or temperature. The closest automated station, Gjögur, located at 31.0 m a.s.l. 9 km east-south-east of the Árnesfjall mountain, was not operative at the time of the failure or during the time range considered (2000–2014).

Results

Morphology and structures of the Móafellshyrna landslide

The highest point of failed debris in the Móafellshyrna source area is at 870 m a.s.l., and the toe of the debris is at 330 m a.s.l., meaning a vertical distance H of 540 m. The horizontal travel distance L is 1320 m, so the Fahrböschung ($\tan^{-1}$ H/L) for the Móafellshyrna landslide is 22°. Overall, the landslide deposits range from fine clay to 1–3 m sized boulders. At the time of the failure, the ground was covered by ~ 20–30 cm of snow.

We will describe here the different morphologies and structures left by all of these processes (Fig. 6).

The detachment zone of the landslide (corresponding to Section 1 in Fig. 3b) is a 665-m-wide topographic bench on the north-western side of the Móafellshyrna Mountain. The failure mass consisted of talus deposits lying against the sub-vertical rockwall of the mountain (Fig. 7a). Only some of the talus deposits slid off the bedrock cliff, as remnants are still perched on a topographic bench in the source area, where ice and snow patches were observable 3 years after the occurrence of the slide (Fig. 7b). Nine days after the occurrence of the landslide, the remnant talus material appeared as rectilinear ice-cemented blocks of debris standing vertically at the edge of the bench (Fig. 7c). Their vertical dimension has been visually estimated to be 15–20 m, and some of them have degraded in place, as they are today still observable in the field and in the aerial images, preserved as mounds of debris (Fig. 7d). The debris deposits at the edge of the bench have an average slope angle of 39°, and a drop in elevation between their surface and their contact with the bedrock of 30 m.

The bedrock of the mountain is dissected by sub-vertical and sub-horizontal systems of fractures, which are pervasive and spaced on the scale of tens of centimetres. This orthogonal discontinuity geometry gives rise to multiple blocks that are prone to topple and fall. Three years after the occurrence of the failure, the bedrock still appeared wet at the headscarp, water springs were observable at the contact between the remnant talus deposits and the bedrock, and ice was visible on the headscarp wall (Fig. 7b). The headscarp is marked by a distinctive red colour, caused by the fine silty clay deposits that compose the matrix of the original talus deposits. The

Fig. 6 The morphology of Móafellshyrna landslide. The main morphological features of the Móafellshyrna landslide. Lighting angle from south

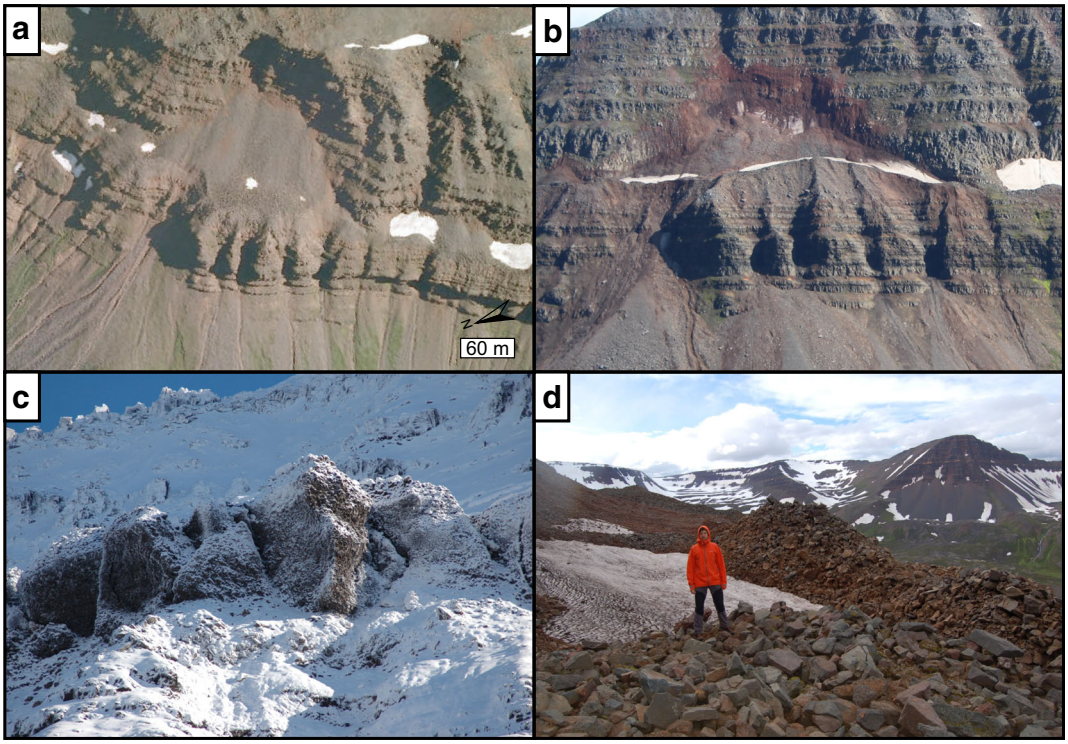

Fig. 7 The geomorphology of the Móafellshyrna landslide's source area. **a** Aerial photograph from 2007 (source samsyn.is) of the source talus deposits lying against the sub-vertical rockwall of the mountain Móafellshyrna Mountain before the landslide**. b** Oblique view of the headscarp of the Móafellshyrna landslide, with remnants of the source deposits lying against the rockwall and perched at the edge of the bench**. c** Unstable blocks of frozen talus deposits perched at the edge of the topographic bench 9 days after the failure. **d** Cones of deposits resulting from the degradation of blocks of ice-rich sediments, perched at the edge of the topographic bench (picture taken in July 2015).

angle of slope of the headscarp, where bedrock is fully or partially exposed, is generally ~ 50° and the slip surface in the source area is upwards concave.

After the initial sliding movement, the debris mass encountered the edge of the topographic bench. The debris mass was transferred through the chutes that are carved in the bedrock cliff below the source area.

Topographically below, the debris mass encountered the 30° talus deposits that are located at elevations of 690 m to 510 m a.s.l. The falling debris mass entrained new material from these talus deposits, and eroded a channel down the middle of the talus slope (Fig. 8b; corresponding to Section 2 in Fig. 3b). Visual estimates from photographs taken a few days after the occurrence of the failure show that the thickness of the talus debris entrained by the initial mass was much higher than the one observed from field inspection 3 years later (3 to 5 m; Fig. 8), and this channel has been partially re-filled by material that fell subsequently down the talus slope.

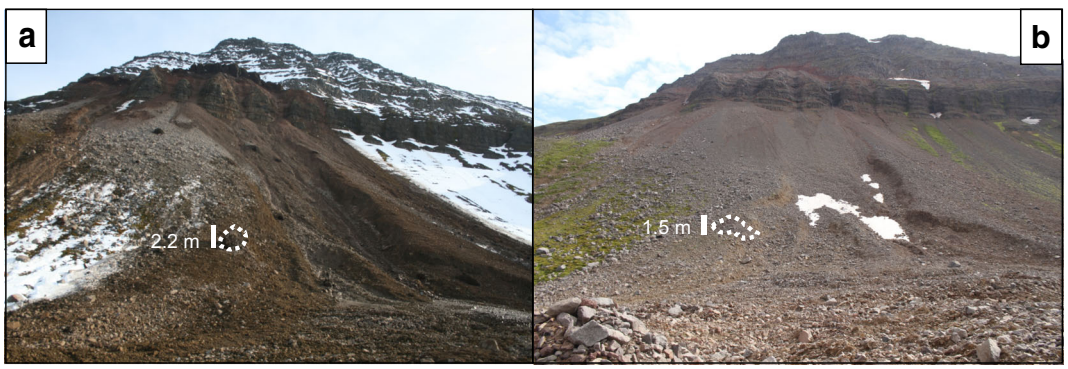

Fig. 8 Entrained talus deposits. **a** The erosional area as result of the entrainment of talus deposits by the initial mass (the picture was taken on 29th September 2012. **b** The same view of the erosional channel, partially re-filled by new talus material (the picture was taken in July 2015). Note the cone of debris as scale, resulting from the degradation of the ice-cemented block in panel **a**

The debris mass then reached a low slope area at the foot of the talus slope, and then proceeded further downslope accumulating deposits in a nearly flat area (Fig. 9a; corresponding to Section 3 in Fig. 3b). In this accumulation area, there are thirteen 11–40-m-long compressional ridges, separated by depressions (Fig. 9b). These compressional ridges are partially parallel to the runout direction of the flow (NW to WNW), but those towards the centre of the accumulation area verge towards NE, probably because the flow encountered a topographic obstacle to the west. The ridges are rounded and sinuous, are 5–10 m wide, and from the bottom of the intra-ridge depressions to the crest of the ridge they are 0.5–1 m high on average (Fig. 9a, b). At the contact between the foot of the talus slope and the accumulation zone, there are lobate features, and discrete zones of well-sorted fine and coarse deposits (Fig. 9a). In this accumulation zone of the landslide, we found 17 cones of debris 4 to 39 m wide and tens of cm to 10 m high. We recognise these cones as molards (Fig. 9c), resulting from the degradation of blocks of ice-cemented talus deposits that were observable a few days after the landslide occurred. In this same zone of the landslide, at the foot of the talus slope, fresh boulders up to 1–3 m high are also present (Fig. 9a). In this accumulation area, a secondary lobe was deposited on the north-eastern side of the landslide, striking N260°. This secondary lobe has a distinctive "fish-tail" shape, characterised by a terminal bifurcation into two lobes (Fig. 9a). The distinct borders of the secondary lateral lobe "fish tail" that deviated laterally from the main runout path of the landslide allowed a better constrained reconstruction of the topography before its deposition. This secondary lateral lobe travelled on a slope of only ~ 12° for 240 m, so with an estimated coefficient of kinetic friction (calculated according to the definition of Heim (1932) and Shreve (1966) as the tangent of the mean slope from the source to the distal margin of a landslide) of approximately 0.21.

Other smaller secondary lobate features are also present further upslope. The lobate deposits have a thickness of 1 m up to 3 m, and have abundant boulders and gravel in a fine (silty clay) matrix. There is a preferential distribution of coarse material towards the edges of the lobe, while fine debris tends to be found towards its centre. From observations made 4 days after the failure, the lobe bulldozed the snow as it travelled downwards on a slope of only 12° (Fig. 9d).

The main debris mass continued in a north-westerly direction and travelled downslope, forming a straight channel. This is a zone where deposits were transferred (corresponding to Section 4 in Fig. 3b), and the thickness of the deposited debris sheet is less than 1 m. This section of the landslide has a channel-form 263 m long

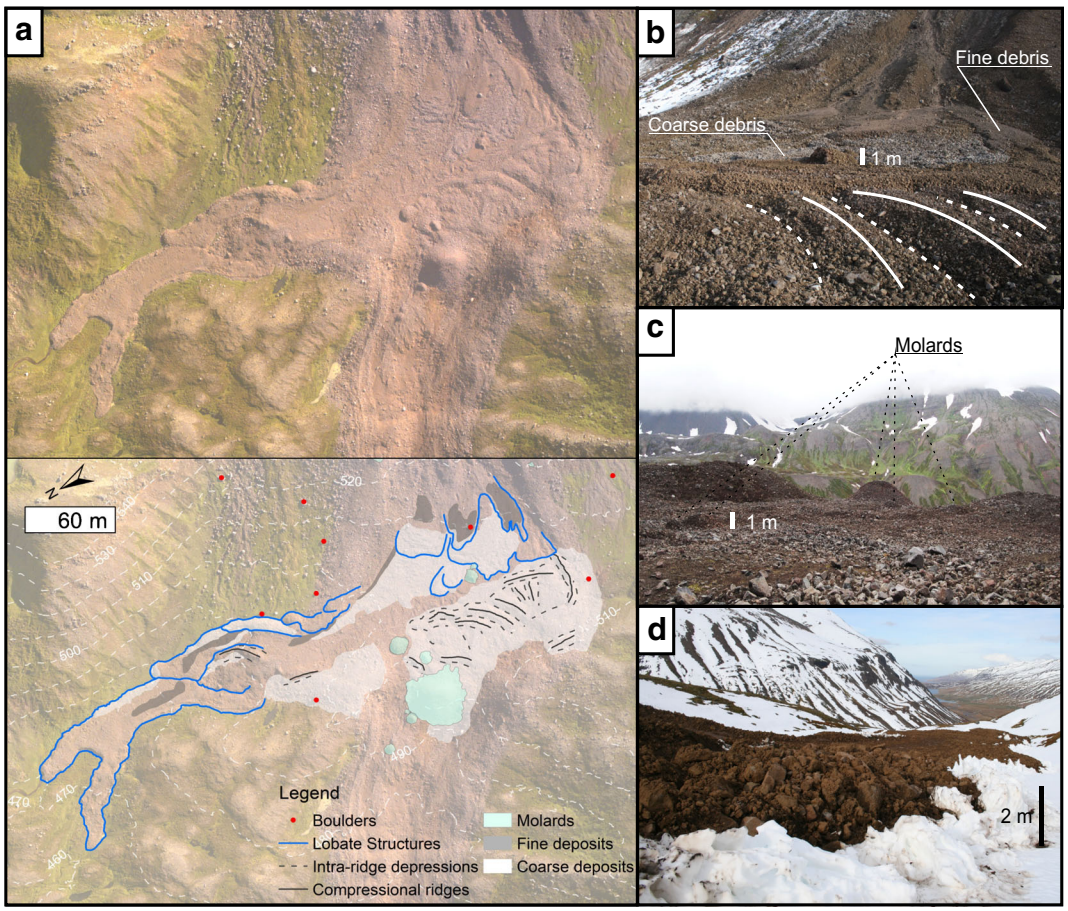

Fig. 9 **a** The main geomorphological features of the upper accumulation zone of the Móafellshyrna landslide. **b** Ridges (crests marked with solid lines) and intra-ridge depressions (white-dashed lines) in the first flat accumulation area encountered by the flow. In the background, discrete zones of coarse debris and lobes of fine debris are present. **c** Some of the cones of debris (molards) scattered on the accumulation area. **d** Snow bulldozed by the "fish tail" lobe (pictures taken 9 days after the landslide)

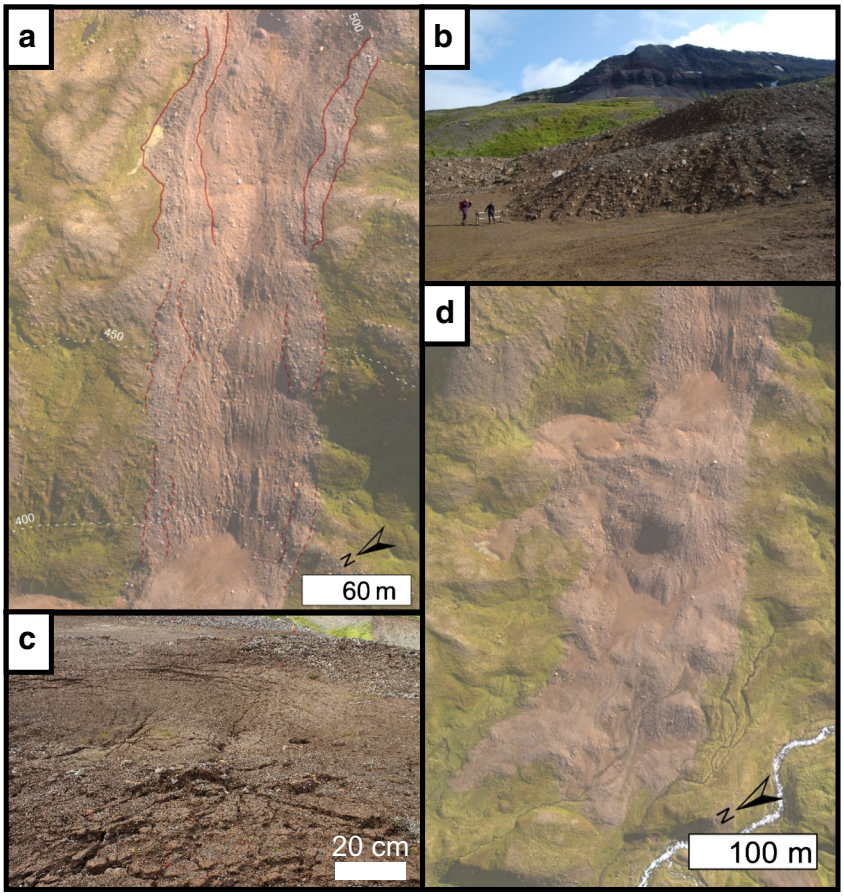

Fig. 10 The channel and the terminal lobe of the Móafellshyrna landslide. **a** The channel has lateral levees (red lines), which are not well defined downwards (dashed red lines). **b** View from south-east of part of the terminal lobe with ridges and furrows and where coarse 23oulder-gravelly deposits are dominant, in contact downslope with an area where silty-clay deposits are dominant. **c** View from south-east of sand boil structures in the terminal lobe. **d** Aerial view of the terminal lobe, with the main zones where fine (silty-clay) and coarse (23oulder-gravelly) debris are dominant

and up to 107 m wide (Fig. 10a). This channel is not observed in the aerial images of the slope before the occurrence of the landslide. In the central part, it is characterised by ridges and furrows with N145° direction. The lateral margins show a different granulometry, being mainly composed by blocks, forming poorly-defined lateral levees (Fig. 10a).

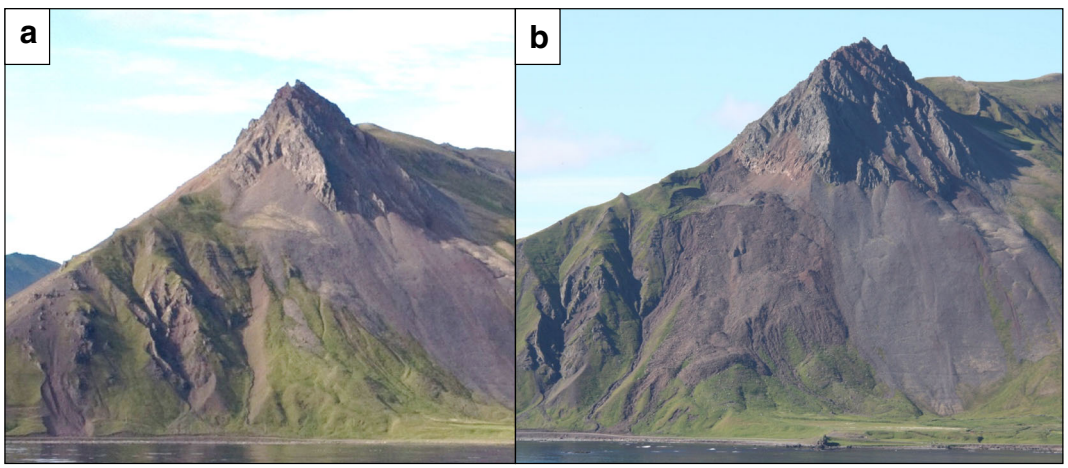

Fig. 11 **a** Oblique view from north-east of the Árnesfjall Peak (picture taken on 13-08-2008, courtesy of Ingvi Stígsson). **b** Olique view from north of the Árnesfjall landslide (picture taken in July 2016)

The debris mass ended its path on a gently sloping surface, almost reaching the Galtará river (Fig. 10d). The flow formed a terminal lobe 369 m long, up to 218 m wide and with a thickness of at most tens of centimetres (10–50 cm). This terminal accumulation zone of the landslide (corresponding to Section 5 in Fig. 3b) is characterised by discrete flat areas where silty to clay material segregated from the gravelly material, sometimes forming secondary lateral lobes with ponded water, or pools of muddy sand. These zones dominated by the fines show "sand boil" structures (4 to 5 m in diameter; Fig. 10c), which result from the liquefaction of water-saturated fine sediment, and cracks a few metres long (1–5 m). Where the topography is steeper, longitudinal ridges and furrows (up to 40 m long) were created by the transport of blocky material.

Morphology and structures of the Árnesfjall landslide

The Árnesfjall landslide detached from the northern flank of the Árnestindur peak at 418 m a.s.l., and its toe extends to the bottom of the valley at 70 m a.s.l., with a lateral debris flow that reached the road (Strandavegur 643) at a few metres above sea level (Fig. 11a, b). The vertical distance H between the top and bottom of the landslide is 348 m, while the horizontal travel distance L was 560 m, giving a Fahrböschung of 32°. The landslide material ranges from clay to large boulders in grain size. Similar to Móafellshyrna, the main failure mass consisted of ice-cemented talus slope deposits, in this case lying against the north-facing, sub-vertical rockwall of the Árnestindur peak (Fig. 11a). Parts of the talus deposits were not mobilised by the landslide and still cover 75,000 m^2 of the northern side of the Árnesfjall Mountain (Fig. 11b). These preserved talus deposits show deformation features, such as transverse fissures (20–50 m long; Fig. 12a) probably due to permafrost creep. The basalt

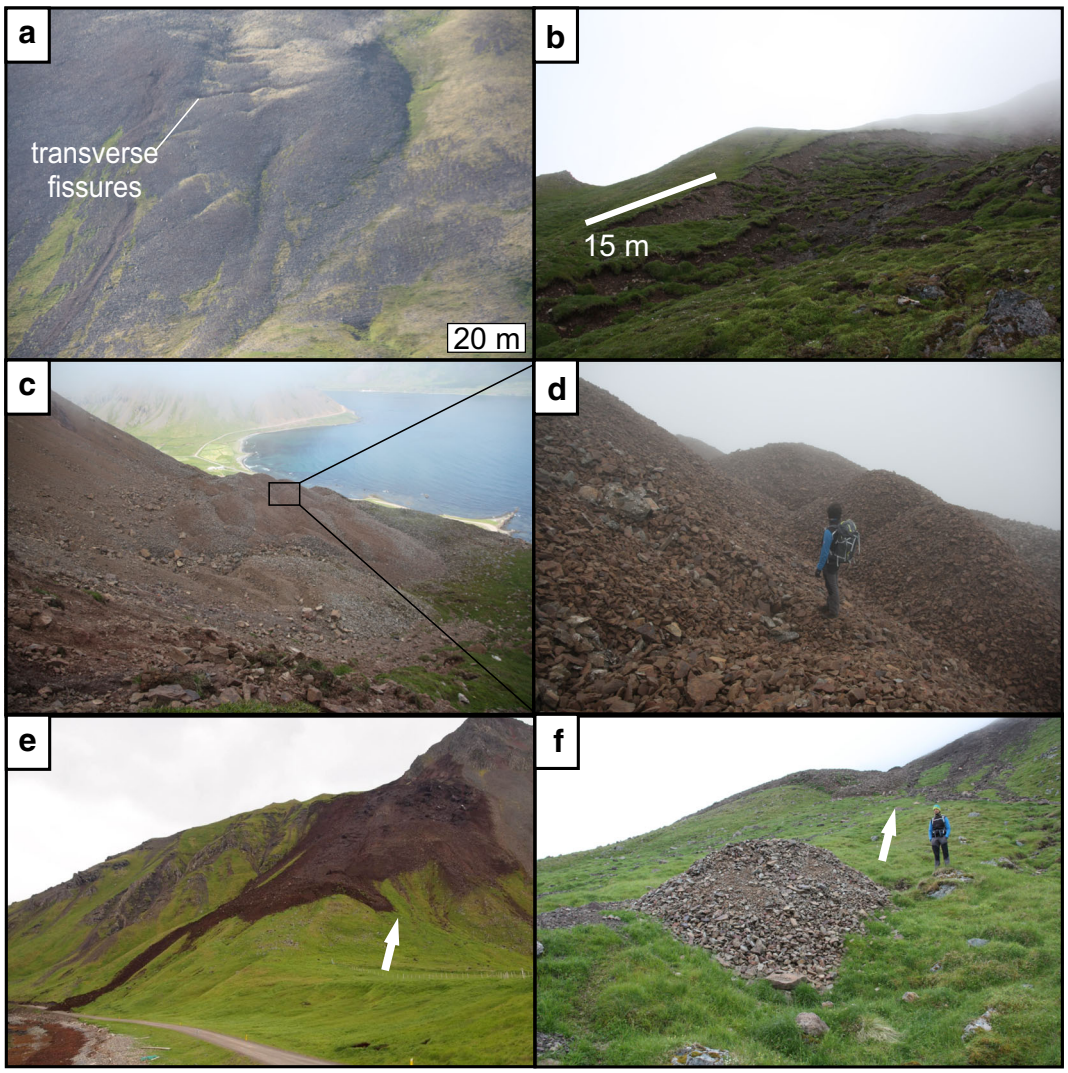

Fig. 12 The morphologies of the Árnesfjall landslide. **a** Reserved talus deposits next to the landslide that show deformation features probably due to permafrost creep. **b** Lateral minor scarps on the eastern side of the landslide. **c** The dense group of elongated molards perched below the headscarp. **d** Molards in the depletion zone are formed by talus deposits and can reach heights of 4 m. **e** A view from the road Strandavegur 643 of the landslide on the day of the failure. Note the square shape of the blocks of ice-rich sediments scattered on the landslide' surface. The white arrow points to the same place as the arrow in the next panel. **f** An isolated molard at the foot of the western debris flow (absent in panel **e**), which developed from an isolated block that fell 2 days after the occurrence of the failure

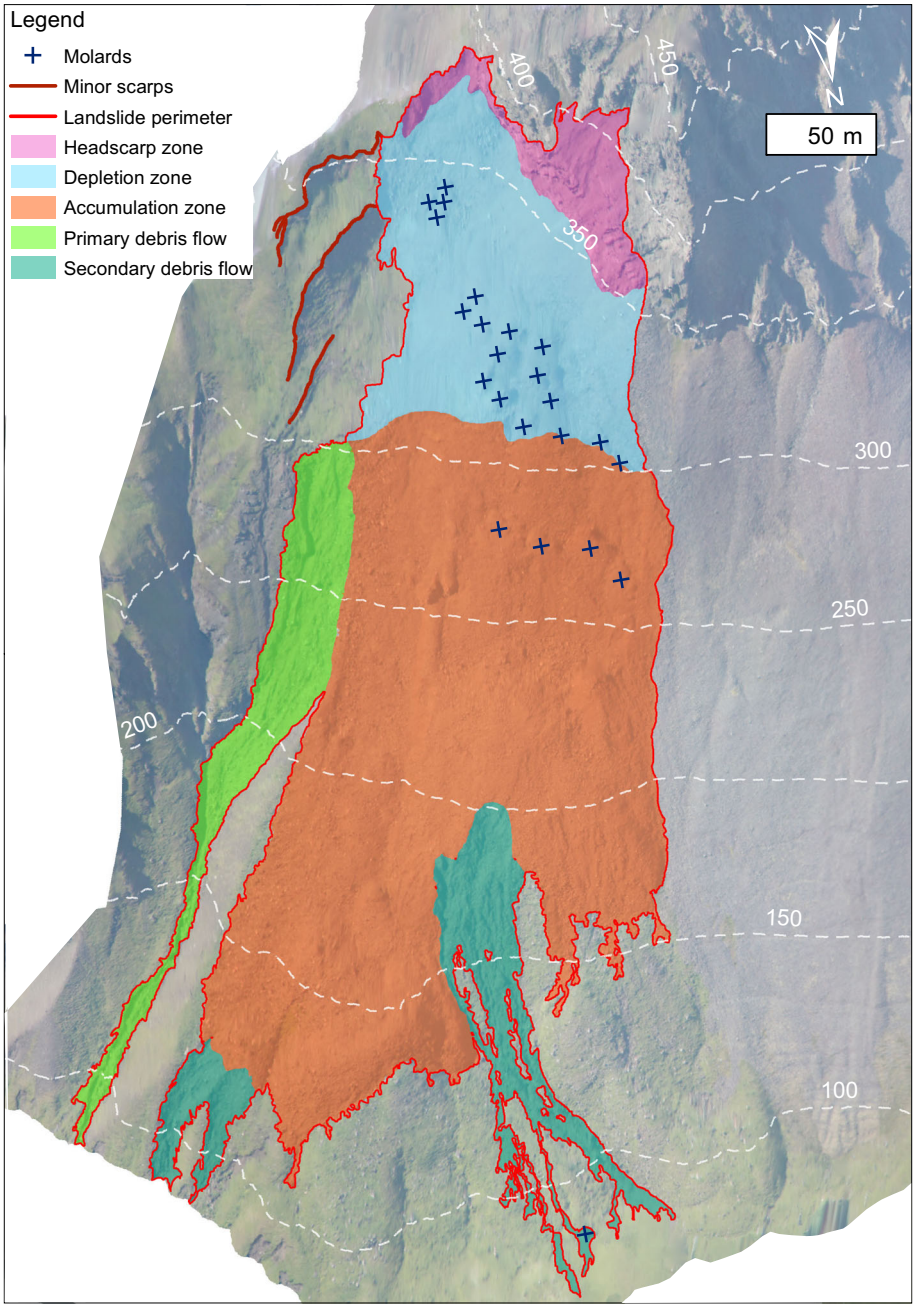

Fig. 13 Map of the main morphological features of the Árnesfjall landslide

composing the bedrock of the mountain displays a pervasive (spaced on the scale of centimetres) primary foliation dipping 30° towards SSW. This is cut by a pervasive discontinuity system (cooling joints) that dips sub-vertically between WNW and ESE, with typical joint spacing of 1–2 m.

In the detachment zone (corresponding to Section 1 in Fig. 5b) on the western side of the landslide, the headscarp has a distinctive red colour due to remnants of fine material composing the matrix of the original talus deposits (Fig. 11b) and an average slope of 49°. On the eastern side, the landslide has three semi-circular and upwards concave minor scarps (50 to 85 m long), forming up to 15-m-thick tilted blocks made from surficial colluvium (Fig. 12b).

In the depletion zone (corresponding to Section 2 in Fig. 5b), the source material was tilted downwards, but parts of the talus deposits are still perched in this area of the landslide (Fig. 12c). In particular, multiple elongated cones of talus deposits lie here (Fig. 12c, d), densely grouped ~ 40–150 m below the top of the headscarp. They are up to 27 m long and almost 4 m high and are the result of the degradation of angular ridges composed of ice-cemented talus deposits that formed during the tilting downwards of blocks of source material during the failure, so they are recognised as molards. Four of these are located in the accumulation area downslope. On the downward-facing surfaces of the cones that are closest to the external edge of the depletion zone,

it is possible to observe lichens; hence, this surface has not been greatly disturbed by the failure: its preservation reflects a rotation of the whole debris mass.

The slope transition between the depletion zone and the accumulation zone is quite abrupt, from an angle of ~ 18° at the edge of the depletion zone, to 33° in the upper part of the accumulation zone. The direction of movement of the whole mass was N58°. The accumulation zone (corresponding to Section 3 in Fig. 5b) is composed in the centre by a relatively uniform debris mass, with debris flows around the periphery (Fig. 12e). The debris mass is 180 wide and 360 m long, and its thickness ranges from 5 m in the upper part to up to 15 m at the toe. It has two central terminal lobes and the eastern lobe ends with two small (66 and 70 m long) debris flows. The deposits are composed of clasts (ranging from 5 cm to tens of centimetres, rarely bigger than 1 m) and gravel, with scarce silty clay matrix. Some isolated molards are scattered on the surface of the debris mass. They are more circular and less elongated than those in the depletion zone, are generally composed of boulder-gravelly material (with a couple of exceptions where they are matrix supported by silty-clay material) and range in height from 20 cm up to rare cases of 1 m.

The debris flow on the northeastern side, which happened at the same time as the landslide, originates at the top of the debris mass (Fig. 13), so spans the whole accumulation zone and then extends to the Strandavegur 643 road. It is 30 m wide at its head, where abundant clasts from 30 to 50 cm up to 1 to 2 m size are present, particularly at the contact with the debris mass. The channel is 1 to 2 m deep and shows 30–50 cm up to 1 m high lateral levees. Secondary debris flows depart the foot of the east side of the accumulation zone as well, reaching the road downslope (Fig. 12e). Other secondary debris flows on the north-northwestern side of the landslide are 224 m long and develop at the terminal edge of the main debris accumulation zone. They bifurcate downslope into two channels less deeply incised (30–60 cm) that have 10 to 30-cm-thick lateral levees. By comparing photos taken the day of the slide and field inspection, we observed that the development of these debris flows occurred between the 10th and 12th July 2014. In the terminal lobe of one of the debris flows, a molard is present (Fig. 12f). This block is not visible in the photos taken on the day of the failure (Fig. 12e), so must have failed after the main landslide event.

Volumes and runout analysis of the Móafellshyrna landslide

Estimations from field observations of the deposit thickness indicate that the volume of debris that was mobilised by the Móafellshyrna landslide was between 295,000 and 440,000 m^3, considering that the landslide covers an area of 293,900 m^2.

We reconstructed the pre-failure topography of the source deposits to quantify the talus deposit volumes that were perched on the topographic bench before the occurrence of the failure. Figure 14 shows the DEM of difference (DoD) for the source area, obtained by subtracting the manually reconstructed pre-failure topographic surface from the post-failure topographic surface. The volume of the talus deposits mobilised out of this area obtained through this calculation is 116,900 m^3. Fifteen- to 20-m-thick debris is still perched at the edge of the bench; hence, this area remains unchanged despite material having been transported through it.

The channel carved in talus deposits below the topographic bench shows that there was entrainment of this material by the source mass, or bulking of the landslide, as also shown in the DoD in Fig. 15, where there is up to 7.8 m of erosion. Assuming that the surrounding talus deposits were not mobilised, we have reconstructed the topography of the talus slope before the failure, calculating the volume of debris eroded by the failing mass. The calculated entrained mass is 110,800 m^3 (Table 3), which corresponds to 35% of the total mobilised material. However, it is likely that the volume entrained was higher, since the visual estimations from the pictures taken a few days after the occurrence of the landslide reveal that the channel was more deeply incised than when the LiDAR data were collected—by at least 1 m on average. This leads to an estimate of roughly 10,000 m^3 extra volume, considering the lower part of the channel where most of the material was eroded.

The calculation of the volumes of the landslide features via (i) differencing the present topography from the reconstructed pre-failure topography and (ii) DEM measurements of the areas where this calculation was not possible, given a total volume of ~ 227,700 m^3 (Table 3).

Table 3 Summary of the parameters for the Móafellshyrna landslide measured in the field and from DEMs

Móafellshyrna landslide measurements	Value	Unit
Whole landslide		
Landslide's horizontal length L	1320	m
Landslide's fall height H	540	m
Fahrböschung	22	°
Average landslide's debris thickness from field estimation	1–1.5	m
Landslide deposit area	257,700	m^2
Landslide's volume from field estimation	257,700–386,000	m^3
Landslide's volume from DoD	227,700	m^3
Source area		
Source area	32,700	m^2
Estimated thickness of remnant source deposits	15–20	m
Source mass volume from DoD	116,900	m^3
Entrainment area		
Entrainment area	17,400	m^2
Length of entrainment area	307	m
Width of entrainment area	66–105	m
Average slope angle of entrainment area	30	°
Estimated thickness of entrained debris	3–5	m
Estimated entrained volume	52,200–87,000	m^3
Entrained volume from DoD	110,800	m^3

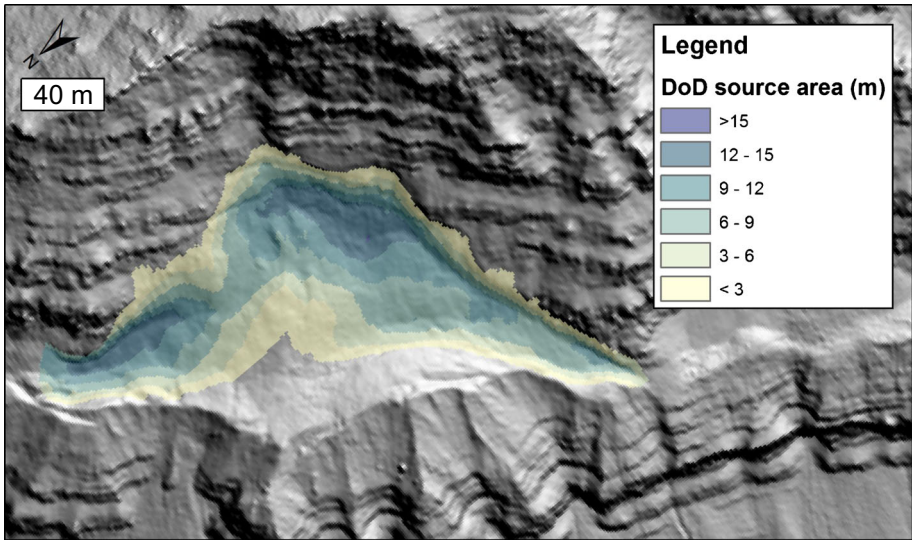

Fig. 14 DEM of difference (DoD) between the post-failure topography (1 m gridded DEM from airborne LiDAR from 2015) and the reconstructed pre-failure topography of the source area of the Móafellshyrna landslide. Background is the LiDAR hillshaded DEM

Runout analysis of molards and boulders of the Móafellshyrna landslide

The blocks of ice-rich sediment that fell at the foot of the talus slope during the Móafellshyrna event were deposited almost intact in their final resting position because ground ice cemented them during transport. To analyse the mobility of the blocks of ice-rich sediment now preserved as molards, we compared the reach angles and the volumes of the debris cones with those of "normal" rock boulders mobilised during the landslide event that fell to the foot of the talus slope via simple rock fall (Fig. 16). The debris cones show both travel distance and volumes consistent with those of boulders involved in common rock-fall processes.

Volumes and runout analysis of the Árnesfjall landslide

Covering an area of 71,700 m^2, the estimated volume mobilised by the Árnesfjall landslide is between 71,700 and 215,000 m^3, considering an average landslide deposit thickness of 1–3 m. The Fahrböschung of the landslide is 32° (Table 4).

The landslide deposits lie on a slope that was once uniformly covered by talus deposits (Fig. 11). Figure 17 shows the DEM of difference (DoD) for the source area (Fig. 17), obtained by subtracting the manually reconstructed pre-failure topographic surface from the post-failure topographic DEM. The volume of erosion calculated from this DoD is 77,400 m^3. The thickness of the debris mantle in the accumulation zone is up to 5 m thick in the upper part, and in the terminal lobe just a few tens of centimetres near the western debris flow. From these field measurements, we estimated a volume of debris deposited in the accumulation zone, excluding the debris flows, to be 55,000–275,000 m^3.

Part of the deposit transported by debris flows was removed by local authorities (because these deposits covered the Strandavegur 643 road). The major part of the deposits of these debris flows is so thin (often few tens of centimetres) that reconstructing the topography before their emplacement is not possible. Less than 500–800 m^3 of debris have been transferred via these debris flows. This volume is negligible in the overall sediment budget of the landslide, but it is important in terms of hazard assessment purposes.

Antecedent weather conditions to the Móafellshyrna landslide

In 2012, in the Móafellshyrna area, the summer and spring were unusually warm, and the autumn was particularly cold. In the town of Ólafsfjörður, the average temperature in July 2012 was

Table 4 Summary of the parameters for the Árnesfjall landslide measured in the field and from DEMs

Árnesfjall Landslide measurements	Value	Unit
Whole landslide		
Landslide's area	71,700	m^2
Landslide's horizontal length L	560	m
Landslide's fall height H	348	m
Fahrböschung	32	°
Average landslide's debris thickness from field estimation	1–3	m
Landslide's volume from field estimation	71,700–215,100	m^3
Source area		
Source area	16,700	m^2
Source mass volume from DoD	77,400	m^3
Accumulation area		
Accumulation area	55,000	m^2
Estimated thickness in accumulation area	1–5	m
Estimated volume in accumulation area	55,000–275,000	m^3

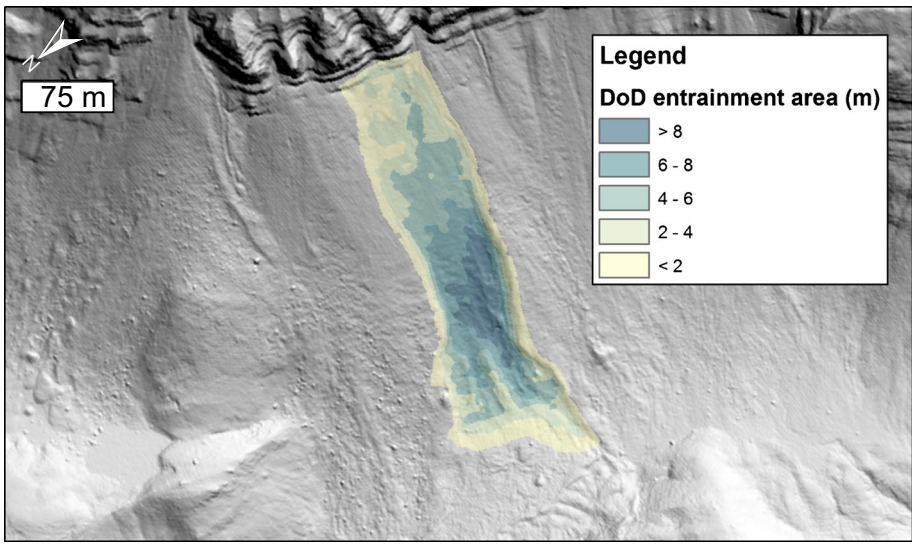

Fig. 15 DEM of difference (DoD) between the post-failure topography (1 m gridded DEM from SfM of post-slide photos controlled to LiDAR data) and the reconstructed pre-failure topography of the entrainment area of the Móafellshyrna landslide. Background is the LiDAR hillshaded DEM

10.4 °C and 10.9 °C in August, when the average temperatures for the same months for the period 2000–2012 are 9.8 °C and 9.6 °C, respectively. In September 2012, the average temperature was 5.7 °C compared to an average of 7.2 °C for 2000–2012 (Fig. 18). Our corrected average daily air temperature at the altitude of the Móafellshyrna event in the days preceding the failure were around − 1 to − 2 °C, meaning also lower night-time temperatures (see Fig. 7 in Sæmundsson et al. (2018) for more detail). Sub-freezing conditions occurred in the evening of 19th September, with a drop below 0 °C in the atmospheric temperature at Öxnadalsheiði weather station, and snow on the ground at the time of the Móafellshyrna landslide confirms sub-zero temperatures in the mountains before the event. Sub-freezing conditions also prevailed at this altitude prior to the event.

During the spring and summer months before the Móafellshyrna landslide, dry conditions were recorded. At the end of the summer, from 20th August to 20th September 400–550 mm of total precipitation fell in the area, which is the equivalent of the average annual precipitation in the town of Ólafsfjörður for the period 2000–2012 (Sæmundsson et al. 2018). When the Móafellshyrna event occurred, 540 mm precipitation had been recorded in the town of Siglufjörður and 490 mm at

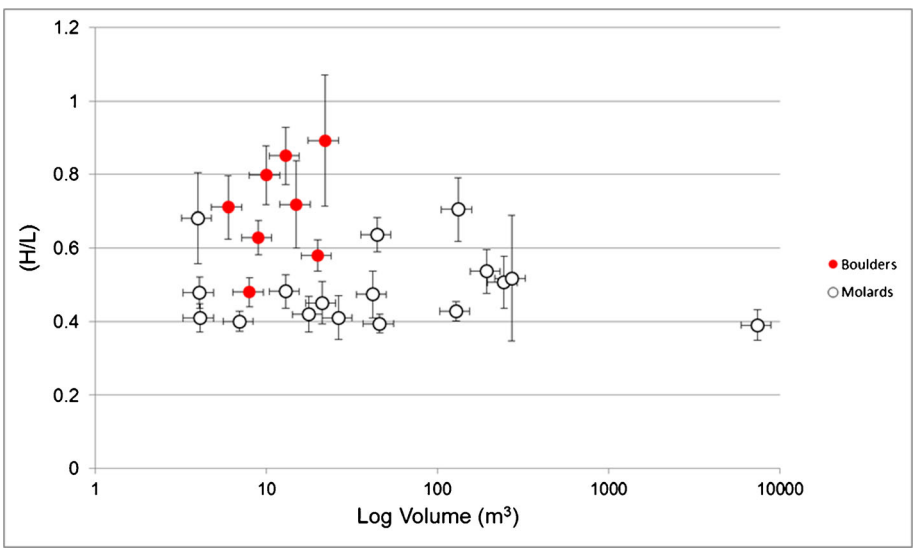

Fig. 16 Semi-logarithmic plot of block and molards volume (m^3) versus the tangent of reach angle (H/L). The vertical error bar is the propagation of errors of L (whose error is the standard deviation of the length of the various potential energy lines of fall) and H (whose error is the thickness of the bedrock cliff for boulders and the thickness of the deposits perched on the topographic bench for the molards in correspondence of the centreline path of fall). The horizontal error bar is calculated using an accuracy of 25% according to Conway and Balme (2014) for molards and is calculated arbitrarily using an accuracy of 20% of field and plan-view measurements for boulders

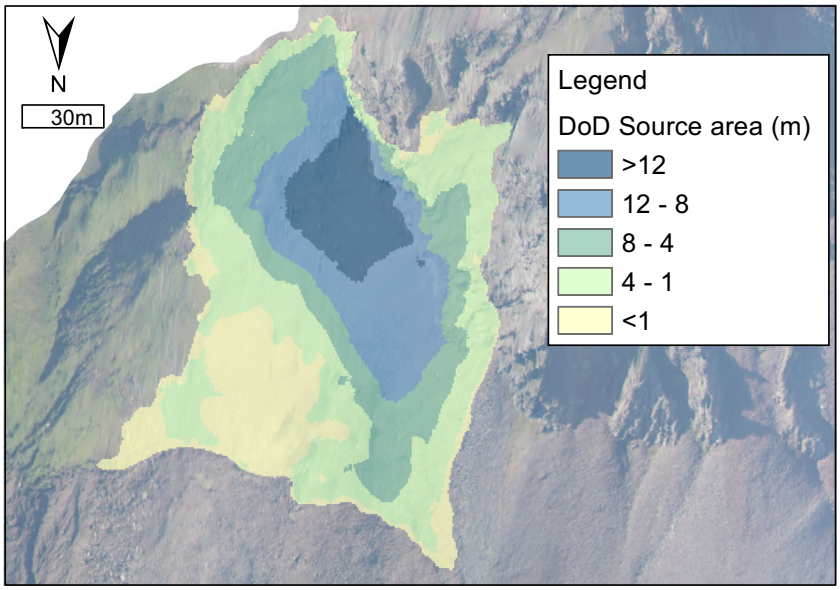

Fig. 17 DEM of difference (DoD) between the post-failure topography (18 cm gridded DEM from ground-based SfM from 2016) and the reconstructed pre-failure topography of the source area of the Árnesfjall landslide

Ólafsfjörður weather stations since 23rd July, which corresponds to 40–45% of the mean annual precipitation from 2000 to 2012 (Fig. 18). September was the month with maximum precipitation for any given year for the period 2000–2012, with a range between 70 and 250 mm.

Antecedent weather conditions to the Árnesfjall landslide

The temperature patterns in 2014 were not unusual for the region nearby Árnesfjall (Fig. 19). The average temperature measured in Litla-Ávík was 9.2 °C in June and 9.8 °C in July in 2014 (Fig. 19a), which are values that fall within the average range recorded for the period 2000–2014 (Fig. 20). The average temperatures for these months for the period 2000–2012 are 7.4 °C and 9.3 °C, respectively. However, on 8th June, 2 days before the occurrence of the Árnesfjall event, the temperature rose from an average of 7.8 °C (temperature recorded the week before), to an average of 11.0 °C from 8th to 10th July (Fig. 19b).

The spring months preceding the Árnesfjall event were dry (Fig. 20). From May to 30th June 2014, dry conditions prevailed in Litla-Ávík. Ten days before the occurrence of the failure, almost 90 mm of rain fell in the area close by the Árnesfjall mountain, of which 62 mm were recorded between 4th and 6th July (Fig. 21). From the beginning of May to 9th July, the cumulative precipitation in Litla-Ávík was 140 mm (Fig. 21). July was the month with the maximum precipitation registered for the year 2014 (Fig. 20), with the peak recorded in the 10 days before the landslide (Fig. 21). The station of Litla-Ávík is positioned on the west-south-western side of the Reykjaneshyrna mountain, and most of the precipitation-carrying winds are north-north-easterly winds (Jónsson et al. 2004), so the orographic part of the precipitation is probably missing for this station, but it would not have been missing at Árnesfjall.

On the day of the event, almost no precipitation occurred (0.2 mm). It is not unusual, and it is well documented in literature, which the onset of landslides can occur from a few hours to a days after intense precipitation (Iverson and Major 1987; Iverson 2000; Matsuura et al. 2008; Baum and Godt 2010). Probably, sudden rainfall, likely more intense than recorded at Litla-Ávík, hit the region near the Árnesfjall Mountain on the preceding day and this could have triggered the landslide.

Discussion

Both the Móafellshyrna and Árnesfjall landslides can be broadly classified as complex landslides, accordingly to Varnes (1978)'s classification. The initial movement occurred on a concave-up surface in the source area. However, both show morphological and morphometric characteristics that suggest other types of movement, due to the nature of the debris material, the topography and the presence of water and ice. In both landslides, the source material was weakly cemented (being formed of ice-cemented talus deposits), and perched on a steep slope, both conditions that can be considered as preconditioning factors for the initiation of rapid mass movements (McColl 2012). Despite similar initial settings, the landslides developed quite differently. We discuss the dynamics of the two landslides individually, then the plausibility of ground ice as a source of fluid for flow-dominate phases of behaviour. Finally, we discuss more general insights into the hazard of landslides related to ground-ice thaw.

The dynamics of the Móafellshyrna landslide

Detailed morphological analysis of the 2012 Móafellshyrna landslide allowed us to infer the emplacement mechanisms. These give important information regarding the initiation, transport, deposition and evolution of the mass movement. We infer that the Móafellshyrna landslide evolved through three different types of dynamics: (i) bedrock constrained rotational debris slide, (ii) rock/debris fall and (iii) debris flow/slide (Fig. 22). The initial movement

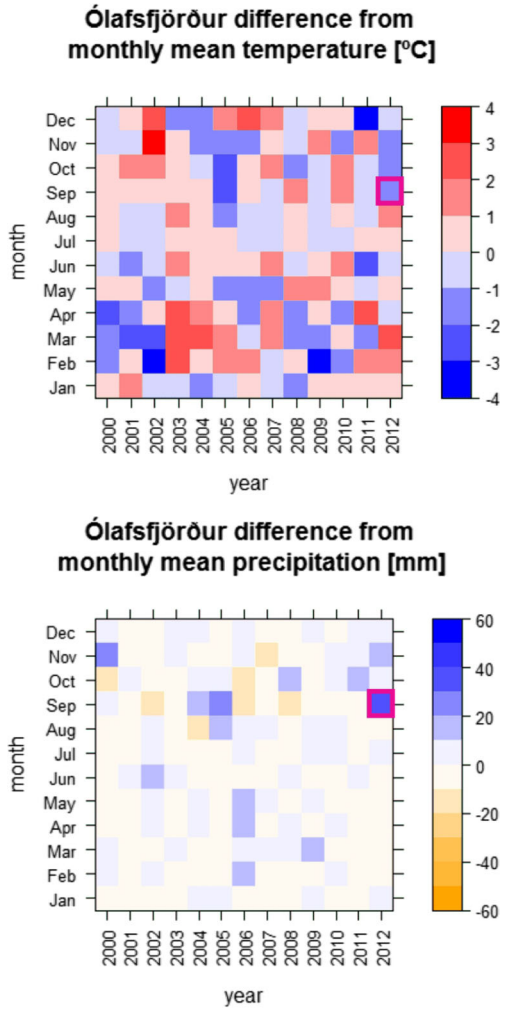

Fig. 18 Matrix plots of the difference between the average monthly temperature (top) and precipitation (bottom) and the average value for that month for the period 2000–2012 for the Ólafsfjörður station (data supplied by the IMO in 2016). The pink squares mark the month of the occurrence of the Móafellshyrna event. Modified after Sæmundsson et al. (2018)

of the Móafellshyrna source material was by sliding along the bedrock surfaces, producing a rotational movement because of the shape of the bedrock surfaces, accompanied at the same time by rock/debris fall. The debris mass fell on the talus cone downslope (Fig. 6b), entraining new material. Some material continued further downslope through a process analogous to debris flow/slide, while some material stalled on the first bench forming secondary lobes. After the deposition of the landslide deposits, prolonged rock/debris fall activity occurred intermittently over time because of the thawing of the ice cementing the perched material.

The bedrock surface underlying the landslide is upward concave, being composed of a steep cliff followed by a sloping bench, forming an ideal sliding geometry to develop a rotational slide. The presence of water at the contact between the talus deposits and the bedrock and of ice on the headscarp wall observed in the field after the event could reflect the presence of groundwater flow that exploits the intersecting discontinuity systems. Once the material had propagated downwards over the cliff, the debris slide entrained the talus material below, a common mechanism in rock and debris slides/avalanches that can cause liquefaction and an increase in flow volume (Hungr and Evans 2004; Geertsema et al. 2006; Huggel et al. 2008). This entrained material must have had a strong impact on the emplacement of the debris, since it comprised at least ~35% of the total volume of the mobilised mass (Table 3). The debris-flow/slide dynamic is also evident in the flat accumulation area below the entrainment zone, where it is likely that debris was transported in a second stage—probably a few minutes after the deposition of the main flow/slide deposits. The geomorphic features created by this second pulse have not been overprinted by newer flows and therefore were the last to form. The ridges and depressions similar to those formed in this zone have been observed in a debris avalanche in British Columbia and have been associated with a water-poor debris (Roberti et al. 2017). Ridges and intra-ridge depressions in Móafellshyrna show that the direction of the movement was affected by the topography and the fluid content. Coarse debris accumulated in this first flat accumulation area, as the debris mass encountered a topographic high (Fig. 9a); this made part of the debris mass deviate to the NW, creating new lobes of debris on a relatively flat surface (5–12°). The secondary lobate features are neatly defined, revealing debris emplacement in sequential pulses after the main mass failure. Furthermore, the "fish-tail" lobe bulldozed surface snow while moving downward on a slope of only 12° (Fig. 9d). This mechanism and the deviation of the debris from the main runout path have, in previous studies, been attributed to differential mobility of debris within the debris mantle, especially in debris avalanches on glacier surfaces (Delaney and Evans 2014). We infer that the more fluid component of the falling mass was instead transferred downwards during the main mass failure, forming the channel characterised at its centre by ridges and furrows—indicating erosion—and lateral levees at its margin—indicating deposition.

The evidence of the fall component of the Móafellshyrna failure is not limited to the boulders now found at the foot of the talus slope below the source area, which fell during the whole Móafellshyrna event and up to months after the occurrence of the landslide, as reported by the residents of the Þrasastaðir farm (Sæmundsson et al. 2018). The isolated molards found scattered at the foot of the talus slope represent blocks of ice-rich deposits that also fell from the source area before degrading at their final resting-place. Coherent blocks were still visible 9 days after the occurrence of the failure, unstably perched at the edge of the topographic bench (Fig. 7c). Some of them were not transported downslope, but degraded in place resulting in indistinct cones of debris preserved in the source area (Fig. 7d). However, the question remains as to how the molards in the accumulation zone came to be there: did they fall or were they pushed? Since the reach angle model is one of the universally recognised methods to analyse travel distance of small rock falls (< 100 m^3), we have compared the reach angle and size of the cones of debris left during the Móafellshyrna event to those of normal boulders that fell in the same area of the landslide (Fig. 16). Normally, "the larger the falling boulder, the smaller the value of the reach angle" (e.g. Corominas 1996; Copons et al. 2009). According to this principle, both boulders and particularly molards in Móafellshyrna show a high mobility. We compared the reach angle and size of the Móafellshyrna molards to those of blocks of similar size in

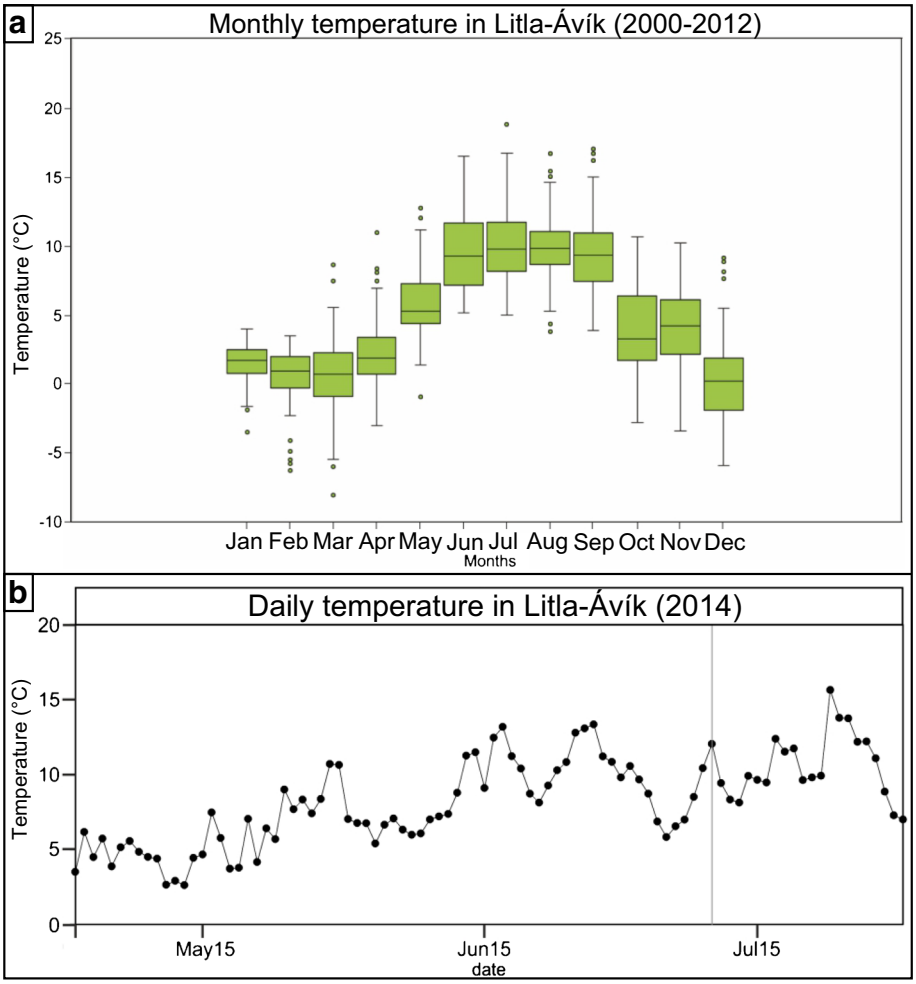

Fig. 19 Temperature data at Litla-Ávík. a A boxplot of the temperature data from the Litla-Ávík station for each month between the years 2000 to 2012 (data supplied by the IMO in 2018). The end of the lines is where the max and min values of temperature were measured for each month, excluding the outliers that are displayed as dots (outliers are defined as values which lie outside 1.5 times the interquartile range above the upper quartile and bellow the lower quartile). The green boxes are where the 50% of accumulated measured precipitation falls and the black lines are the medians of each month. b Daily temperature data from the Litla-Ávík (LTAV) weather station for the months of May, June and July 2014 (data supplied by the IMO in 2018). The vertical bar is the date of the Árnesfjall event

Spain, where Copons et al. (2009) found that the rock fall size has a strong influence on the travel distance also for block size < 10^5 m^3 (Fig. 23). Copons et al. (2009) plotted individual block volumes and the farthest boulders found at the study area, since they represent the largest volumes and largest travel distances from past rock falls at the same site. They found a negative relationship between block volume and the reach angle ratio value. Both boulders and molards in Móafellshyrna have high mobility, but consistent with the mobility of 'normal' rock-fall boulders analysed by Copons et al. (2009). In the case of molards, their higher mobility could also be partially attributed to a 'compound' transport mechanism, as it is possible that, once fallen, they landed on the still mobile landslide debris material. They might then have been rafted on the surface of a viscous flow (as shown by the compressional ridges) and transported to greater distances.

The fluid-dominated phase of the Móafellshyrna landslide is evident in the landforms downslope of the flat accumulation area. The presence of sand-boil structures in the terminal lobe of the landslide could be an indicator of liquefaction, as similar features were observed in analogous landslides (for example in the Frank landslide in Alberta; McConnell and Brock 1902) and attributed to liquefaction (Xu et al. 2012). In the same area of the landslide, segregation of coarse and fine material in discrete zones is observed, and probably occurred due to the fines leaking out of accumulations of coarse material in topographic traps. The presence of a straight channel with poorly defined lateral levees, and of a terminal lobe with coarse and fine deposits in discrete zones, could also be related to a fluid-dominated phase, similar to a debris flow/slide (Costa 1984). The fluid component of the failing mass overshot the flat accumulation area and even crossed a slight topographic high, and then flowed along the line of steepest descent. The transition from a rock/debris slide to a debris flow is a common process that has been related to liquefaction (Voight and Sousa 1994; Vallance and Scott 1997; Capra and Macías 2000; Crosta 2001; Boultbee et al. 2006; Xu et al. 2012; Tost et al. 2014). A source of fluid was necessary for producing saturation and to transfer of material downslope. There are two possible sources of fluid that caused the evolution of the Móafellshyrna landslide into a debris flow/slide-like mass movement. The first could have come from the fluid saturating the debris material before it was mobilised. Abundant

precipitation preceded the Móafellshyrna event, so it is likely that the talus material both on and below the topographic bench was saturated. It is possible that the initial falling debris mass encountered the talus slope below the topographic bench, and that here the fluid phase separated from the solid-dominated phase and slid further downwards, as it was more mobile. This is a common process that has been reported in other debris slides/avalanches (Hungr and Evans 2004; Geertsema et al. 2006; Huggel et al. 2008; Haeberli et al. 2017; Roberti et al. 2017). The separation of a fluid-dominated phase from a dry phase has also been reproduced by two-phase numerical modelling (Pudasaini 2012; Pudasaini and Krautblatter 2014). The second possible source of fluid could have been the thawing of the ground ice cementing the source debris material. Furthermore, in rock-ice avalanches on snow-covered glaciers, ice and snow are thought to reduce the friction by 50% (Schneider et al. 2011b; Sosio et al. 2012). The presence of a thin (few tens of centimetres) layer of snow on ground at the time of the failure could have helped lubricate the movement, even if its role was minor considering that in most rock-ice avalanches, the path material entrained is snow or ice, which is not the case for Móafellshyrna.

To summarise the evolution of the Móafellshyrna landslide, the failure developed through four different chronological steps:

- Step 1: Slide and rock/debris fall: The source mass formed by ice-cemented talus deposits detached and slid over the bedrock with a rotational component. Because of an abrupt topographic jump, the source talus debris disaggregated and was transferred downslope through the process of rock/debris fall.
- Step 2: Debris entrainment: The source mass then encountered a talus slope lying below the topographic bench, entrained part of the talus deposits and moved further downslope. Once the debris mass reached the first flat accumulation area, the landslide material divided into two different rheology types: solid-dominated and fluid-dominated.
- Step 3a: Fluid-dominated phase: The fluid dominated phase was transferred downslope and produced forms similar to those of a debris flow/slide, such as sand-boil structures, leveed channels and a terminal lobe with segregation of coarse and fine material in discrete zones.
- Step 3b: Solid-dominated phase: The solid dominated phase left thick (up to metres) coarse debris ridges and depressions that show the direction of the movement. It also produced secondary lobes—one of which bulldozed the snow covering the ground at the time of the failure—which show a granular behaviour and reveal debris emplacement in sequential pulses after the main mass failure.
- Step 5: Rock/debris fall: Rock and debris fall processes occurred onto the landslide body when it was still mobile and rafted small boulders and blocks of ice-cemented talus landing on its surface. The fall activity continued for months (probably even years) after its occurrence.

The dynamics of the Árnesfjall landslide

Similarly to the Móafellshyrna landslide, the Árnesfjall landslide initiation and emplacement involved different dynamic processes. In Fig. 24, the sequence of the different processes that occurred during the Árnesfjall failure is illustrated. The initial movement of the source material was by rotational sliding, accompanied at the same time by lateral debris flows. After the deposition of the landslide, a secondary set of debris flows occurred, accompanied by the transport of an 'outrunner' (nearly intact blocks of debris that detach from a submarine landslide body (De Blasio et al. 2006), the term is also used for terrestrial landslides (Milana 2016).

The initial downslope rotational sliding movement is indicated by the distinctive curved slip surface in the scarp zone. The presence of elongated conical ridges of loose deposits (molards), which were cemented by ground ice at the time of the failure, are evidence of rotational-sliding motion, since they appear to be produced by *en echelon* concave-upward rupture surfaces (rotated ice-cemented ridges of debris). As opposed to Móafellshyrna, the molards in Árnesfjall sometimes preserve the original stratification of the talus deposits, and on the downwards-facing surfaces of the most downslope molards, there are lichens, evidence that the debris material was tilted downwards as a single mass. This process was only possible in talus material because the ground ice gave the loose debris a more rigid rheology. Similar conical features in debris slides that formed through an analogous process

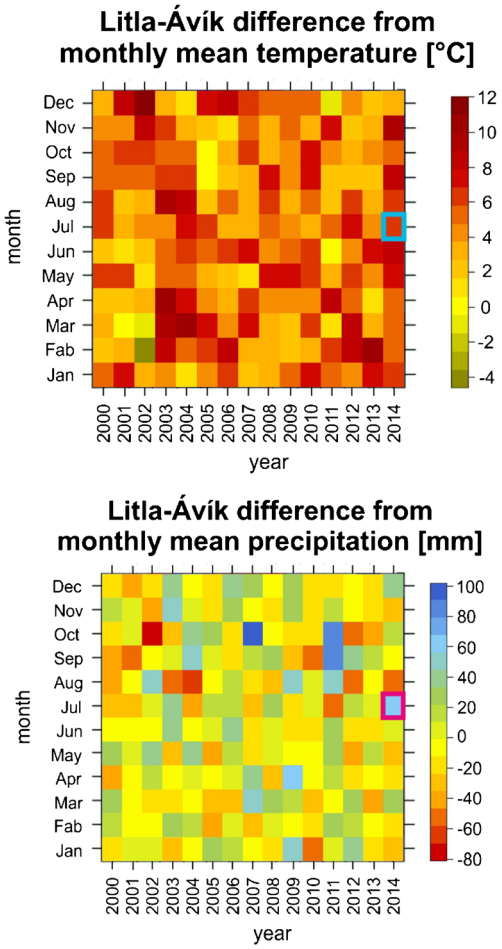

Fig. 20 Matrix plots of the difference between the average monthly temperature (top) and precipitation (bottom) and the average value for that month for the period 2000–2014 for the Litla-Ávík station (data supplied by the IMO in 2018). The blue and pink square marks the month of the occurrence of the Árnesfjall event

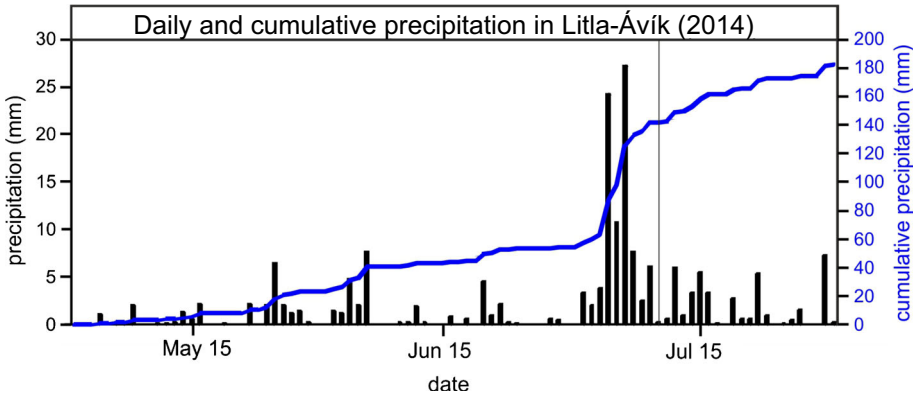

Fig. 21 Daily precipitation (black bars) and cumulative precipitation (blue lines) for precipitation measurements from the Litla-Ávík weather station for the months of May, June and July 2014 (data obtained from IMO in 2018). The vertical bar is the date of the Árnesfjall event

were observed by Brideau et al. (2009) in the Little Salmon Lake debris slide, Canada, where ice-rich deposits were transported by the surrounding sliding saturated material. Furthermore, most of the molards lie in the depletion zone, which is separated from the accumulation zone by an abrupt transition in slope. This subdivision is typical of rock/debris slides (Varnes 1978) and the Árnesfjall landslide shows a Fahrböschung of 32° that is consistent with debris slides.

The Árnesfjall landslide shows a different dynamic at its periphery, where debris material was mobilised as debris flows, which have lateral levees and terminal lobes. This is not an uncommon characteristic of debris slides, but the presence of secondary debris flows indicates the renewed presence of fluid saturating the material after the initial landslide. The eastern debris flow has the same length as the accumulation zone and follows a channelised morphology that was already present at the time of the failure. It is therefore likely that this debris flow developed contemporaneously with the debris slide, and the pre-existing channel acted as a preferential path for the fluid component of the failing mass. We have shown that the western debris flow developed subsequently to the debris slide, likely triggered by the degradation of the ground ice within the material mobilised by the failure, providing fluid for sediment transport downslope. At the same time (or soon before or after), a block of ice-rich sediment rolled and slid downslope and arrived at repose in the terminal lobe of the debris flow, subsequently degrading to form a molard. In this terminal lobe, the debris are only up to 30–50 cm thick and are dispersed in multi-directional flow lines, so it is expected that this thin sheet of debris was produced by the degradation of the ground ice that was cementing the source material at the time of the failure.

Plausibility of ground ice as a source of water for fluidization

The total potential energy (PE) released by the falling mass in Móafellshyrna is 1.80×10^{12} J. This can be calculated using Eq. 1

$$\mathrm{PE} = \Delta z g \gamma V \tag{1}$$

where Δz is the vertical distance between the centres of gravity (arbitrarily estimated following Lucchitta 1978), g is the gravitational constant, γ is the unit weight of the material and V is the volume mobilised (Erismann and Abele 2001). This PE is calculated assuming an average density of 1863 kg/m^3. This density is obtained by considering 80% of the failed

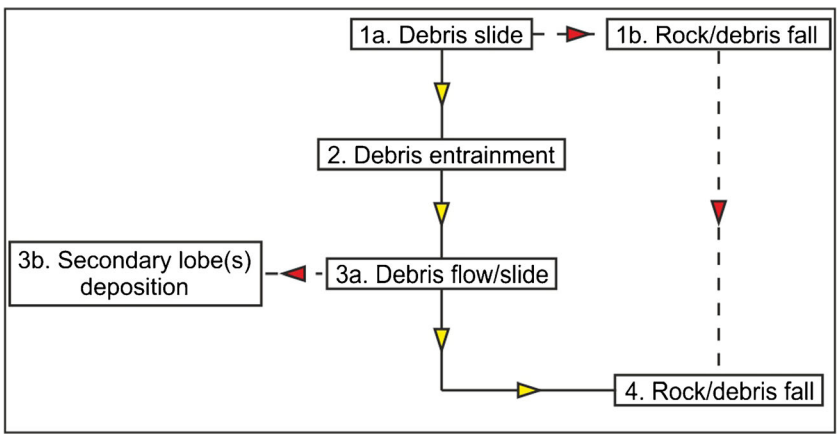

Fig. 22 Flow chart summarising the different processes that occurred during the Móafellshyrna landslide. The arrows in yellow indicate continuous and consecutive processes, while the dashed red arrows indicate intermittent and/or non-consecutive processes. Time goes from top to bottom of the diagram

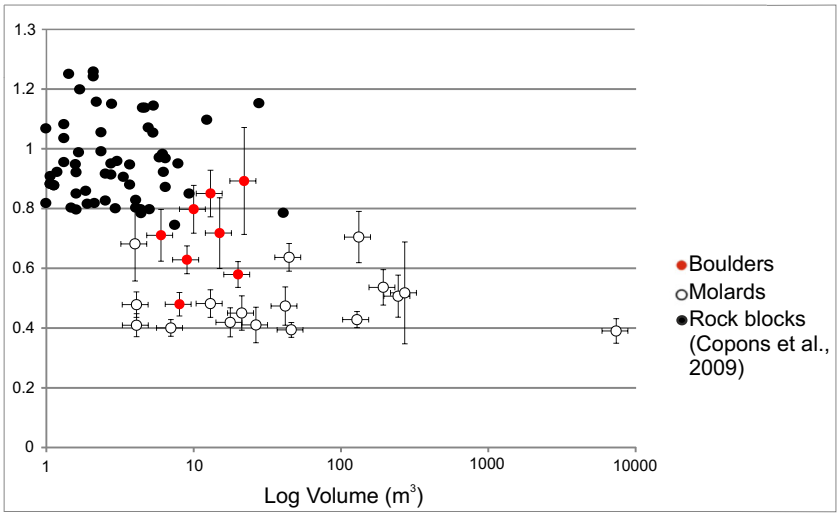

Fig. 23 Semilogarithmic plot of volume (m^3) versus reach angle for the molards and boulders of Móafellshyrna landslide (error bars are the same for Fig. 16) and reach angle of individual rock blocks from Copons et al. (2009).

mass having a density of an average granular flow (2100 kg/m^3; Iverson 1997), and 20% of the mass having the density of ice (917 kg/m^3). This assumption is based on the content of ground ice that was visually estimated at the time of the failure. Knowing the potential energy, it is possible to estimate the amount of ice melt through transmission of energy generated by the falling ice-cemented debris mass. Theoretically, the impact energy of the Móafellshyrna landslide could have melted up to 5.4 × 10^3 m^3 of ice (assuming 3.35 × 10^5 J/kg necessary for melting ice at 0 °C). If we assume that the fluid content of the landslide was coming only from the source material (116,900 m^3), this would lead to a maximum estimate of meltwater of ~ 2.7 × 10^3 m^3 (since blocks of ice-rich sediments had ground ice preserved in the source area and in the landslide body). An extensive amount of energy is dissipated during the collapse, fall and impact of the material, so the actual amount of energy available to melt is probably less. However, the available energy produced by the failure was sufficient to melt the ground ice within the initial slide sediments and could also have plausibly impacted the talus slope below the source area and caused an increase in temperature that generated a further source of fluid from the thawing of the ground ice.

Ground ice and fluid: synthesis of its role in the Móafellshyrna and Árnesfjall landslide dynamics

We infer that the morphological and dynamic complexity of the Móafellshyrna and Árnesfjall landslides—both characterised by various forms related to different gravitational process—is due to the role of thawing-ground ice. Specifically, the two landslides show dynamics analogous to those of rock- /debris-ice avalanches. Relatively low ground-ice concentrations (~ 20%) plausibly contributed to flow-type behaviour in both case studies. There were two sources of liquid that changed the emplacement of the Móafellshyrna and Árnesfjall failures to a flow like movement: the entrainment of saturated material from the talus slope in Móafellshyrna and the fluid for ground-ice thaw in both of the landslides. Heavy prolonged precipitation in Móafellshyrna probably caused the saturation of both the source material and the talus material below the source area, providing enough fluid to cause a transition to a debris-flow emplacement. In Móafellshyrna, the energetics of the landslide were sufficient to melt ground ice. The closest analogue for debris slides that mobilise ice-rich material are rock-ice avalanches. It is known that rock-ice avalanches have 20–35% higher mobility than rock avalanches of the same magnitude in non-glacial settings (Evans and Clague 1988; Huggel

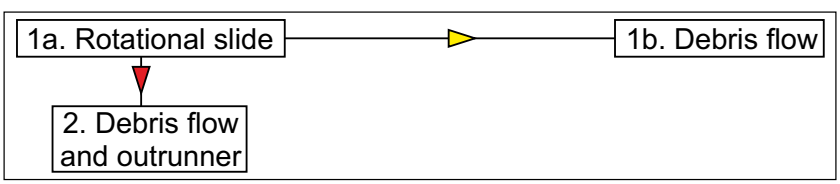

Fig. 24 Flow chart summarising the different processes that occurred during the Árnesfjall landslide. The arrow in yellow indicates time continuous and consecutive processes, while the dashed red arrows indicate intermittent and/or non-consecutive processes

et al. 2005; Schneider et al. 2011a; Sosio et al. 2012). This enhanced mobility is attributed to fluidisation, caused by the reduction of granular friction due to ice melting, basal lubrication by frictional heating of ice (Evans and Clague 1988; Davies and McSaveney 2012) and internal mass and momentum exchange (Pudasaini and Krautblatter 2014). Laboratory experiments with a rotating drum show that the ice in a moving mass of a gravel affects the mobility of the mass as the thaw of that ice supplies water to the flow (Schneider et al. 2011b). In particular, the friction coefficient of a granular moving mass containing ice decreases linearly with increasing ice content, as also shown to be the case in numerical modelling (Sosio et al. 2012). A volume of ice in the mixture greater than 40% causes an increase in pore-water pressure and liquefaction, consequently generating a transition from a dry granular mass to a debris flow-like movement, and eventually to a hyperconcentrated flow (De Blasio and Elverhøi 2008; Schneider et al. 2011b; De Blasio 2014; Schneider et al. 2011c; Sosio et al. 2012). However, laboratory studies do not consider the scale effects introduced by ice on the friction angle—Schneider et al. (2011b) recognise a stronger dependence on ice content for mixtures with larger grains; this could have important implications for natural scale events.

These two landslides add to the relatively sparse field evidence that it is appropriate to consider rock- and debris-ice avalanches as a useful analogy for the less studied ones involving thawing ground ice, in particular exhibiting transitions in behaviour from movement as a dry granular mass to a debris flow-like movement. The mobility of these types of mass movement can change during their propagation due to entrainment of ice, snow and substrate material; such mixing with the source material can reduce the friction coefficient, altering the runout (McSaveney 1978; Evans and Clague 1988; Schwab et al. 2003; Huggel et al. 2005; Sosio et al. 2012). In general, the mobility of rock/debris slides/avalanches is not affected by their volume, but is mainly controlled by the availability and distribution of a source of liquid along their path (Hungr and Evans 2004). Greater mobility is predicted for rock/debris avalanches interacting with ice during propagation than for those that do not. De Blasio (2014) lists as characteristics of landslides affected by icy conditions and lubrication "strong stretching, longitudinal stripes, long runout, outrunner blocks, digitations, and marked spread of the landslide". Tongue-shaped deposits, digitate margins and minor surface relief—features similar to those found in wet snow avalanches—are found in rock/debris avalanches involving ice or propagating on ice surfaces (Sosio 2015). Similarly, Árnesfjall and Móafellshyrna propagated on rough terrains and divided into several lobes.

We infer that ground ice profoundly influenced the morphology and dynamics of the Móafellshyrna and Árnesfjall landslides and have played a role in their triggering. Low temperatures prior to the event combined with the snow cover are evidence that sudden influx of water from precipitation was not the trigger for the Móafellshyrna landslide. Permafrost degradation is confirmed by the recent studies of Sæmundsson et al. (2018) and Czekirda et al. (2019). The recent study of Sæmundsson et al. (2018) discusses that the landslide originated because of the lubrication of the talus material at its base and consequent loss of cohesion derived by deep permafrost thaw. The authors also suggest that the thaw was probably enhanced by heat propagation and warmer water input from the bedrock-southern side to the northern side. In Czekirda et al. (2019), a transient permafrost model was used to model ground temperature evolution in Iceland for the last six decades (1960–2016), finding out that the extension of permafrost in the country has significantly decreased in 2010–2016 in comparison to previous decades. Permafrost is warm (average ground temperatures above – 2 °C) and is present mainly in the Tröllaskagi peninsula, where lower permafrost limits are modelled at 600–900 m a.s.l. at windy sites and at 1000–1150 m a.s.l. in snow-rich areas. The model was also run using site-specific parameters for both the Móafellshyrna and Árnesfjall sites, where ground temperature warming for the source areas was predicted, particularly since years 2000s. In Móafellshyrna, the modelled ground temperatures show a long-term warming and a decrease in the depth of permafrost base around the time of the failure. In the case of Árnesfjall landslide, sudden and heavy precipitation occurred 10 days before the occurrence of the landslide, after a spring dominated by dry conditions. At this location, the annual trend of temperature does not seem to differ from the past years. According to an Icelandic technical report (Sigfússon et al. 2016), in the period 1949–1992 and 1995–2015 for the Gjögur and Litla-Avik stations, there were more than 150 frost days per year, but 4 months (December–March) had an average temperature below the freezing point. The combination of sudden and probably intense precipitation, and an abrupt rise of temperature up to 12.5 °C in the days before the failure could have caused the degradation of the ground ice present in the source area, which is a combination of factors that have been attributed to the release of rapid mass movements elsewhere worldwide (Huscroft et al. 2003; Crosta et al. 2004; Huggel et al. 2005). At Árnesfjall, shallow permafrost of ~ 1 m was present until 2000, but Czekirda et al. (2019) warn that the smaller solar radiation received by north-facing slopes was not accounted for, and the modelling period might have been too short.

Implications for hazard and risk

The dynamics of both Móafellshyrna and Árnesfjall landslides are complex and this can raise problems when evaluating potential hazard. Their complexity is a result of several factors, such as topography, the entrainment of new saturated material in the case of Móafellshyrna and the nature of the source material, composed of talus deposits cemented by ground ice. In Árnesfjall, two different mechanisms (rotational slide and debris flow) characterised the development of the landslide, while in Móafellshyrna, there were three (slide, debris flow/slide and rock/debris fall). The fall and debris-flow activities following both the main failures suggest that ground-ice thaw can cause slope instability to continue even after the landslide event and therefore increase their related hazard. Models of the dynamics of rapid flow slides, debris flows and avalanches can accurately predict the runout extensions whenever the rheological parameters are well defined (e.g. McDougall and Hungr 2004), but they are not yet able to accurately handle the complexity of dynamics exhibited by landslides involving ground ice, whose presence should be accounted for whenever considering hazard. This because entrainment and dynamic loading of water saturated sediments can enhance the mobility of landslide material (Abele 1997; Crosta et al. 2009) and be dominant

factors in the hazard cascade (Walter et al. 2020). Landslides like the Móafellshyrna and the Árnesfjall ones are more difficult to characterise and model, and this can generate problems when predicting similar rapid mass movements in analogous settings. The dynamics of rock avalanches entraining large quantities of saturated debris have been examined through numerical modelling, showing that this type of complex landslide behaves in manner transitional between rock avalanche and debris avalanche (Hungr and Evans 2004). Real runouts of rock avalanches in permafrost environments have been shown to exceed predicted ones by 30%, probably because of fluidization processes (Bottino et al. 2002). Clusters of large, highly mobile rock avalanches sourcing from bedrock ridges in probable permafrost zones have been identified in the last few years over decennial periods of records, and they occurred after long-term trend of warm air temperatures, suggesting that ice loss due to permafrost degradation could have induced larger failures and could have been the dominant factor contributing to their occurrence (Coe et al. 2018; Bessette-Kirton and Coe 2020). The hazard and associated risk in permafrost areas from landslides may extend notably further from their source areas than in non-permafrost ones, and an increase in frequency of this type of slope failures should be carefully considered.

Conclusions

Landslides involving loose debris cemented by ground ice are largely unreported, but have the potential to cause casualties if they impact inhabited regions. Primarily by using morphological analysis, we are able to make a number of inferences about the dynamics of the Móafellshyrna and Árnesfjall landslides, two failures that occurred in the last decade in northern Iceland and that mobilised ground-ice cemented talus deposits.

1. The dynamics of both landslides were complex, and the nature of the movement evolved during the event, changing the mobility and trajectories of the landslides. Both initiated as a slide over a bedrock surface, but field evidence is presented for components of rock/debris fall, a sliding motion evolving to a more dispersive debris slide/avalanche motion, a failing mass becoming more mobile due to liquefaction and being emplaced as a debris flow/slide, and secondary debris flows activated as a result of thaw of the ground ice, which originally cemented the source material. Thus, the complexity of the morphological features of these landslides reveals that mass movements involving ground ice can be multi-phase, comprising a fluid dominated phase and a solid-dominated phase that can consist of multiple pulses.
2. The fluid-dominated phase could derive from two sources, namely the entrainment of additional saturated material and the thawing of ground ice.
3. The presence of ice has enhanced the mobility of the mass movements, and ground ice thawing caused a more complex propagation of the failure, with a debris flow-like final evolution.
4. Ground-ice thawing-induced failures could cause slope instability—such as fall and debris flow—to continue even after the landslide event, and therefore increase the related hazard.
5. In terms of evaluating hazards and risk, such landslides involving a notable flow phase might be more common than expected from the literature, as the ground ice can completely degrade by the time that the landslide is surveyed, and thus may impact farther from their sources than expected.>

These complex types of landslides might be more common than reported in the literature: if such failures are not witnessed during the event and surveyed immediately afterwards, the evidence for the former presence of ground ice can have disappeared by the time that the landslide deposits are surveyed. The inferences in this paper will therefore almost certainly apply to other similar mass movements involving terrains affected by degrading ground ice. Given the potential for rapid degradation of mountain permafrost environments driven by ongoing changes in global climate, obtaining a better understanding of the complex dynamics of these landslides is a vital first step to building a robust hazard assessment should potential source regions exist in, or close to, inhabited areas.

Acknowledgements

This work has been funded by a postgraduate studentship grant (NE/L002493/1) from the CENTA Doctoral Training Partnership funded by the UK Natural Environment Research Council (NERC) and the British Geological Survey University Funding Initiative Studentship (GA/14S/024, Ref: 284). We thank the Natural Environment Research Council Airborne Research Facility (NERC ARF), their Data Analysis Node (NERC-ARF-DAN) and the European Facility for Airborne Research (EUFAR) for air photography and LiDAR data. Thanks go to NERC Geo-physical Equipment Facility (GEF) for the Loans 1048 and 1064 through which differential GPS surveys were possible. C. Morino and S.J. Conway are funded by the Agence Nationale de la Recherche in the framework of the project ANR-19-CE01-0010 PERMOLARDS. We acknowledge the financial support from Région Pays de la Loire, project GeoPlaNet (convention No 2016-10982). C. Jordan publishes with permission of the Executive Director of BGS. We gratefully acknowledge the contribution of our field assistants Francesco Giuntoli, Silvia Crosetto and Sydney Gunnarson. We would like to thank two unanimous reviewers, whose comments have greatly improved the quality of the paper.

Funding This work has been funded by a postgraduate studentship grant (NE/L002493/1) from the CENTA Doctoral Training Partnership funded by the UK Natural Environment Research Council (NERC) and the British Geological Survey University Funding Initiative Studentship (GA/14S/024, Ref: 284); the Agence Nationale de la Recherche in the framework of the project ANR-19-CE01-0010 PERMOLARDS; the Région Pays de la Loire, project GeoPlaNet (convention No 2016-10982).

Data availability All data are freely available under request to the corresponding author.

Code availability NA

Declarations

Competing interests The authors declare no competing interests.

References

Abele G (1974) Bergsturze in den Alpen. Ihre Verbreitung, Morphologie und Folgeerscheinungen. Wiss Alpenvereinshefte 25:230

Abele G (1997) Rockslide movement supported by the mobilization of groundwater-saturated valley floor sediments. Zeitschrift für Geomorphol 1–20

Allen SK, Cox SC, Owens IF (2011) Rock avalanches and other landslides in the central Southern Alps of New Zealand: a regional study considering possible climate change impacts. Landslides 8:33–48. https://doi.org/10.1007/s10346-010-0222-z

Andrés N, Tanarro LM, Fernández JM, Palacios D (2016) The origin of glacial alpine landscape in Tröllaskagi Peninsula (North Iceland). Cuad Investig Geográfica 42:341. https://doi.org/10.18172/cig.2935

Andrés N, Palacios D, Sæmundsson Þ et al (2019) The rapid deglaciation of the Skagafjörður fjord, northern Iceland. Boreas 48:92–106. https://doi.org/10.1111/bor.12341

Andrews JT, Hardardóttir J, Helgadóttir G, E. Jennings A, Geirsdóttir Á, Sveinbjörnsdóttir ÁE, Schoolfield S, Kristjánsdóttir GB, Micaela Smith L, Thors K, Syvitski JPM (2000) The N and W Iceland shelf: insights into last glacial maximum ice extent and deglaciation based on acoustic stratigraphy and basal radiocarbon AMS dates. Quat Sci Rev 19:619–631. https://doi.org/10.1016/S0277-3791(99)00036-0

Arnalds Þ, Sauermoser S, Jóhannesson T, Grímsdóttir T (2001) Hazard zoning for Siglufjörður. Reykjavík

Ashastina K, Schirrmeister L, Fuchs M, Kienast F (2017) Palaeoclimate characteristics in interior Siberia of MIS 6-2: First insights from the Batagay permafrost mega-thaw slump in the Yana Highlands. Clim Past 13:795–818. https://doi.org/10.5194/cp-13-795-2017

Baum RL, Godt JW (2010) Early warning of rainfall-induced shallow landslides and debris flows in the USA. Landslides 7:259–272. https://doi.org/10.1007/s10346-009-0177-0

Beniston M, Farinotti D, Stoffel M, Andreassen LM, Coppola E, Eckert N, Fantini A, Giacona F, Hauck C, Huss M, Huwald H, Lehning M, López-Moreno JI, Magnusson J, Marty C, Morán-Tejéda E, Morin S, Naaim M, Provenzale A, Rabatel A, Six D, Stötter J, Strasser U, Terzago S, Vincent C (2018) The European mountain cryosphere: a review of its current state, trends, and future challenges. Cryosph 12:759–794. https://doi.org/10.5194/tc-12-759-2018

Bessette-Kirton EK, Coe JA (2020) A 36-year record of rock avalanches in the Saint Elias Mountains of Alaska, with implications for future hazards. Front Earth Sci 8:293

Bottino G, Chiarle M, Joly A, Mortara G (2002) Modelling rock avalanches and their relation to permafrost degradation in glacial environments. Permafr Periglac Process 13:283–288. https://doi.org/10.1002/ppp.432

Boultbee N, Stead D, Schwab J, Geertsema M (2006) The Zymoetz River rock avalanche, June 2002, British Columbia, Canada. Eng Geol 83:76–93. https://doi.org/10.1016/j.enggeo.2005.06.038

Brideau M, Stead D, Hopkinson C et al (2009) Preliminary description and slope stability analyses of the 2008 Little Salmon Lake and 2007 Mt . Steele landslides , Yukon. Yukon Explor Geol:119–134

Brynjólfsson S, Schomacker A, Ingólfsson Ó (2014) Geomorphology and the Little Ice Age extent of the Drangajökull ice cap, NW Iceland, with focus on its three surge-type outlets. Geomorphology 213:292–304. https://doi.org/10.1016/j.geomorph.2014.01.019

Capra L, Macías JL (2000) Pleistocene cohesive debris flows at Nevado de Toluca Volcano, central Mexico. J Volcanol Geotherm Res 102:149–167. https://doi.org/10.1016/S0377-0273(00)00186-4

Clague JJ, Huggel C, Korup O, Mcguire B (2012) Climate change and hazardous processes in high mountains. Rev la Asoc Geológica Argentina 69:328–338. https://doi.org/10.5167/uzh-77920

Coe JA, Bessette-Kirton EK, Geertsema M (2018) Increasing rock-avalanche size and mobility in Glacier Bay National Park and Preserve, Alaska detected from 1984 to 2016 Landsat imagery. Landslides 15:393–407

Conway SJ, Balme MR (2014) Decameter thick remnant glacial ice deposits on Mars. Geophys Res Lett 41:5402–5409. https://doi.org/10.1002/2014GL059980.Received

Copons R, Vilaplana JM, Linares R (2009) Rockfall travel distance analysis by using empirical models (Soì a d ' Andorra la Vella , Central Pyrenees). Nat Hazards Earth Syst Sci 9:2107–2118. https://doi.org/10.5194/nhess-9-2107-2009

Coquin J, Mercier D, Bourgeois O, Decaulne A (2019) A paraglacial rock-slope failure origin for cirques: a case study from Northern IcelandDes mouvements de masse paraglaciaires à l'origine des cirques : une étude de cas au nord de l'Islande. Géomorphologie Reli Process Environ 25:117–136. https://doi.org/10.4000/geomorphologie.13057

Corominas J (1996) The angle of reach as a mobility index for small and large landslides. Can Geotech J 33:260–271

Costa JE (1984) Physical geomorphology of debris flows. Dev Appl Geomorphol:268–317

Crochet P, Jóhannesson T (2011) A data set of gridded daily temperature in Iceland, 1949–2010. Jökull 61:1–17

Crochet P, Jóhannesson T, Jónsson T, Sigurðsson O, Björnsson H, Pálsson F, Barstad I (2007) Estimating the spatial distribution of precipitation in Iceland using a linear model of orographic precipitation. J Hydrometeorol 8:1285–1306. https://doi.org/10.1175/2007JHM795.1

Crosta GB (2001) Failure and flow development of a complex slide: the 1993 Sesa landslide. Eng Geol 59:173–199. https://doi.org/10.1016/S0013-7952(00)00073-9

Crosta GB, Chen H, Lee CF (2004) Replay of the 1987 Val Pola Landslide, Italian Alps. Geomorphology 60:127–146. https://doi.org/10.1016/j.geomorph.2003.07.015

Crosta GB, Imposimato S, Roddeman D (2009) Numerical modelling of entrainment/deposition in rock and debris-avalanches. Eng Geol 109:135–145

Cruden DM, Varnes D (1996) Landslide types and processes. In: Transportation research board UNRC (ed) Landslides investigation and mitigation. Special Re. Washington, DC, pp 36–75

Czekirda J, Westermann S, Etzelmüller B, Jóhannesson T (2019) Transient modelling of permafrost distribution in Iceland. Front Earth Sci 7:1–23. https://doi.org/10.3389/feart.2019.00130

Davies TRH, McSaveney MJ (2012) Mobility of long-runout rock avalanches. In: Landslides: Types, Mechanisms and Modeling. Cambridge University Press, pp 50–58

De Blasio FV (2014) Friction and dynamics of rock avalanches travelling on glaciers. Geomorphology 213:88–98. https://doi.org/10.1016/j.geomorph.2014.01.001

De Blasio FV, Elverhøi A (2008) A model for frictional melt production beneath large rock avalanches. J Geophys Res Earth Surf 113:1–13. https://doi.org/10.1029/2007JF000867

De Blasio FV, Engvik LE, Elverhøi A (2006) Sliding of outrunner blocks from submarine landslides. Geophys Res Lett 33:8–11. https://doi.org/10.1029/2005GL025165

Decaulne A (2001) Dynamique des versants et risques naturels dans les fjords d'Islande du nord-ouest, l'impact géomorphologique et humain des avalanches et des debris flows, PhD Thesis. University of Clermont II, France

Decaulne A, Sæmundsson P, Pétursson O (2005) Debris flow triggered by rapid snowmelt: A case study in the Gleidarhjalli area, northwestern Iceland. Geogr Ann Ser A Phys Geogr 87:487–500. https://doi.org/10.1111/j.0435-3676.2005.00273.x

Delaney KB, Evans SG (2014) The 1997 Mount Munday landslide (British Columbia) and the behaviour of rock avalanches on glacier surfaces. Landslides 11:1019–1036

Draebing D, Krautblatter M, Dikau R (2014) Interaction of thermal and mechanical processes in steep permafrost rock walls: a conceptual approach. Geomorphology 226:226–235. https://doi.org/10.1016/j.geomorph.2014.08.009

Einarsson MÄ (1984) Climate of Iceland. orld Surv Climatol 15:673–697

Erismann TH, Abele G (2001) Dynamics of rockslides and rockfalls. Springer-Verlag, Berlin

Etzelmüller B, Farbrot H, Guðmundsson Á, Humlum O, Tveito OE, Björnsson H (2007) The regional distribution of mountain permafrost in Iceland. Permafr Periglac Process 18:185–199. https://doi.org/10.1002/ppp.583

Evans SG, Clague JJ (1988) Catastrophic rock avalanches in glacial environments. In: Bonnard C (ed) Landslides - Proceedings of the Fifth International Symposium on Landslides, Lausanne, Switzerland. Lausanne, Switzerland, pp 1153–1158

Farbrot H, Etzelmüller B, Guðmundsson Á, Humlum O, Kellerer-Pirklbauer A, Eiken T, Wangensteen B (2007a) Rock glaciers and permafrost in Tröllaskagi, northern Iceland. Zeitschrift für Geomorphol 51:1–16. https://doi.org/10.1127/0372-8854/2007/0051S2-0001

Farbrot H, Etzelmüller B, Schuler TV et al (2007b) Thermal characteristics and impact of climate change on mountain permafrost in Iceland. J Geophys Res 112:F03S90. https://doi.org/10.1029/2006JF000541
Fischer L, Kääb A, Huggel C, Noetzli J (2006) Geology, glacier retreat and permafrost degradation as controlling factors of slope instabilities in a high-mountain rock wall: the Monte Rosa east face. Nat Hazards Earth Syst Sci 6:761–772. https://doi.org/10.5194/nhess-6-761-2006
Fonstad MA, Dietrich JT, Courville BC, Jensen JL, Carbonneau PE (2013) Topographic structure from motion: a new development in photogrammetric measurement. Earth Surf Process Landforms 38:421–430. https://doi.org/10.1002/esp.3366
French HM (2007) The periglacial environment, Third Edit
Furukawa Y, Ponce J (2010) Accurate, dense, and robust multiview stereopsis. IEEE Trans Pattern Anal Mach Intell 32:1362–1376. https://doi.org/10.1109/TPAMI.2009.161
Garcia S, Arnaud NO, Angelier J, Bergerat F, Homberg C (2003) Rift jump process in Northern Iceland since 10 Ma from40Ar/39Ar geochronology. Earth Planet Sci Lett 214:529–544. https://doi.org/10.1016/S0012-821X(03)00400-X
Geertsema M, Hungr O, Schwab JW, Evans SG (2006) A large rockslide - debris avalanche in cohesive soil at Pink Mountain, northeastern British Columbia, Canada. Eng Geol 83:64–75. https://doi.org/10.1016/j.enggeo.2005.06.025
Geirsdóttir A, Miller GH, Axford Y, Olafsdottir S (2009) Holocene and latest Pleistocene climate and glacier fluctuations in Iceland. Quat Sci Rev 28:2107–2118. https://doi.org/10.1016/j.quascirev.2009.03.013
Glade T (2005) Linking debris-flow hazard assessments with geomorphology. Geomorphology 66:189–213. https://doi.org/10.1016/j.geomorph.2004.09.023
Glade T, Jensen EH (2004) Recommendations for landslide hazard assessments in Bolungarvik and Vesturbyggd, NW-Iceland. Reykjavik
Gruber S, Haeberli W (2007) Permafrost in steep bedrock slopes and its temperature-related destabilization following climate change. J Geophys Res Earth Surf 112:1–10. https://doi.org/10.1029/2006JF000547
Haeberli W, Noetzli J, Arenson L, Delaloye R, Gärtner-Roer I, Gruber S, Isaksen K, Kneisel C, Krautblatter M, Phillips M (2011) Mountain permafrost: development and challenges of a young research field. J Glaciol 56:1043–1058. https://doi.org/10.3189/002214311796406121
Haeberli W, Schaub Y, Huggel C (2017) Increasing risks related to landslides from degrading permafrost into new lakes in de-glaciating mountain ranges. Geomorphology 293:405–417. https://doi.org/10.1016/j.geomorph.2016.02.009
Heim A (1932) Landslides and human lives, N. Skermer. Bi-Tech Publishers, Vancouver, B.C.
Hsu K (1975) Catastrophic debris streams (sturzstroms) generated by rockfalls. Geol Soc Am Bull 86:129–140
Huggel C, Zgraggen-Oswald S, Haeberli W, Kääb A, Polkvoj A, Galushkin I, Evans SG (2005) The 2002 rock/ice avalanche at Kolka/Karmadon, Russian Caucasus: assessment of extraordinary avalanche formation and mobility, and application of QuickBird satellite imagery. Nat Hazards Earth Syst Sci 5:173–187. https://doi.org/10.5194/nhess-5-173-2005
Huggel C, Gruber S, Caplan-Auerbach S, et al (2008) The 2005 Mt. Steller, Alaska, rock-ice avalanche: a large slope failure in cold permafrost
Huggel C, Clague JJ, Korup O (2012) Is climate change responsible for changing landslide activity in high mountains? Earth Surf Process Landforms 37:77–91. https://doi.org/10.1002/esp.2223
Hungr O (1990) Momentum transfer and friction in the debris of rock avalanches: Discussion. Can Geotech J 27:697–697
Hungr O, Evans SG (2004) Entrainment of debris in rock avalanches: an analysis of a long run-out mechanism. Bull Geol Soc Am 116:1240–1252. https://doi.org/10.1130/B25362.1
Hunter G, Fell R (2003) Travel distance angle for "rapid" landslides in constructed and natural soil slopes. Can Geotech J 40:1123–1141. https://doi.org/10.1139/t03-061
Huscroft C, Lipovsky PS, Bond JD (2004) Permafrost and landslide activity: case studies from southwestern Yukon Territory. Yukon Explor Geol 2003:107–119
Iverson RM (1997) The Physics of Debris Flows. Rev Geophys 3:245–296
Iverson RM (2000) Landslide triggering by rain infiltration. Water Resour Res 36:1897–1910. https://doi.org/10.1029/2000WR900090
Iverson RM, Major JJ (1987) Rainfall, groundwater flow, and seasonal motion at Minor Creek landslide, northwestern California: Physical interpretation of empirical relations. Geol Soc Am Bull 99:579–594. https://doi.org/10.1130/0016-7606(1987)99<579:RGFASM>2.0.CO;2
James MR, Robson S (2012) Straightforward reconstruction of 3D surfaces and topography with a camera: accuracy and geoscience application. J Geophys Res Earth Surf 117:1–17. https://doi.org/10.1029/2011JF002289
James MR, Robson S (2014) Mitigating systematic error in topographic models derived from UAV and ground-based image networks. Earth Surf Process Landforms 39:1413–1420. https://doi.org/10.1002/esp.3609
Javernick L, Brasington J, Caruso B (2014) Modeling the topography of shallow braided rivers using Structure-from-Motion photogrammetry. Geomorphology 213:166–182. https://doi.org/10.1016/j.geomorph.2014.01.006
Jóhannesson H (2014) Geological Map of Iceland. Bedrock Geology. Scale: 1:600 000. In: 2nd Ed. Náttúrufræðistofnun Íslands – Icelandic Inst. Nat. Hist. www.arcgis.com/home/item.html?id=c56c70100e21467891fde8f534da96c3#overview
Jónsson HB, Norðdahl H, Pétursson HG (2004) Myndaði Berghlaup Vatnsdalshóla? Náttúrufræðingurinn 72(72):129–138
Kellerer-Pirklbauer A, Lieb GK, Avian M, Carrivick J (2012) Climate change and rock fall events in high mountain areas: numerous and extensive rock falls in 2007 at Mittlerer Burgstall, central Austria. Geogr Ann Ser A, Phys Geogr 94:59–78
King LC (1953) Canons of landscape evolution. Geol Soc Am Bullettin 64:721–752
Krautblatter M, Funk D, Günzel FK (2013) Why permafrost rocks become unstable: a rock-ice-mechanical model in time and space. Earth Surf Process Landforms 38:876–887. https://doi.org/10.1002/esp.3374
Lacelle D, Bjornson J, Lauriol B (2010) Climatic and geomorphic factors affecting contemporary (1950-2004) activity of retrogressive thaw slumps on the Aklavik plateau, Richardson mountains, NWT, Canada. Permafr Periglac Process 21:1–15. https://doi.org/10.1002/ppp.666
Legros F (2002) The mobility of long-runout landslides. Eng Geol 63:301–331. https://doi.org/10.1016/S0013-7952(01)00090-4
Lewkowicz AG, Harris C (2005) Morphology and geotechnique of active-layer detachment failures in discontinuous and continuous permafrost, northern Canada. Geomorphology 69:275–297. https://doi.org/10.1016/j.geomorph.2005.01.011
Lilleøren KS, Etzelmüller B, Gärtner-Roer I, Kääb A, Westermann S, Guðmundsson Á (2013) The distribution, thermal characteristics and dynamics of permafrost in Tr??llaskagi, Northern Iceland, as Inferred from the Distribution of Rock Glaciers and Ice-Cored Moraines. Permafr Periglac Process 24:322–335. https://doi.org/10.1002/ppp.1792
Lindeberg T (2012) Scale invariant feature transform
Lowe G (2004) Sift-the scale invariant feature transform. Int J 2:2
Lucchitta BK (1978) A large landslide on Mars. Bull Geol Soc Am 89:1601–1609. https://doi.org/10.1130/0016-7606(1978)89<1601:ALLOM>2.0.CO;2
Lyle RR, Hutchinson DJ, Preston Y (2004) Landslide processes in discontinuous permafrost, Little Salmon Lake (NTS 105L/1 and 2), south-central Yukon. Yukon Explor Geol:193–204
Lyle RR, Brideau M, Lipovsky P, Hutchnson DJ (2014) Landslides on ice-rich slopes – a geohazard in a changing climate. In: 4th Canadian Conference on Geohazards. ep 10
Magnin F, Josnin JY, Ravanel L, Pergaud J, Pohl B, Deline P (2017) Modelling rock wall permafrost degradation in the Mont Blanc massif from the LIA to the end of the 21st century. Cryosphere 11:1813–1834. https://doi.org/10.5194/tc-11-1813-2017
Matsuura S, Asano S, Okamoto T (2008) Relationship between rain and/or meltwater, pore-water pressure and displacement of a reactivated landslide. Eng Geol 101:49–59. https://doi.org/10.1016/j.enggeo.2008.03.007
McColl ST (2012) Paraglacial rock-slope stability. Geomorphology 153:1–16
McConnell RG, Brock RW (1902) Report on the great landslide at Frank, Alberta, Canada. Can Dep Inter Annu Rep
McDougall S, Hungr O (2004) A model for the analysis of rapid landslide motion across three-dimensional terrain. Can Geotech J 41:1084–1097. https://doi.org/10.1139/t04-052
McSaveney MJ (1978) Sherman glacier rock avalanche, Alaska, USA. In: Developments in Geotechnical Engineering. pp 197–258
Micheletti N, Chandler JH, Lane SN (2015a) Structure from motion (SfM) Photogrammetry. Geomorphol Tech (online Ed London, Br Soc Geomorphol 2.2:303–334. https://doi.org/10.1007/978-1-84882-935-0_7
Micheletti N, Chandler JH, Lane SN (2015b) Investigating the geomorphological potential of freely available and accessible structure-from-motion photogrammetry using a smartphone. Earth Surf Process Landforms 40:473–486. https://doi.org/10.1002/esp.3648
Milana JP (2016) Molards and their relation to landslides involving permafrost failure. Permafr Periglac Process 27:271–284. https://doi.org/10.1002/ppp.1878
Morino C, Conway SJ, Sæmundsson Þ, Helgason JK, Hillier J, Butcher FEG, Balme MR, Jordan C, Argles T (2019) Molards as an indicator of permafrost degradation and landslide processes. Earth Planet Sci Lett 516:136–147. https://doi.org/10.1016/j.epsl.2019.03.040
Patton AI, Rathburn SL, Capps DM (2019) Landslide response to climate change in permafrost regions. Geomorphology 340:116–128. https://doi.org/10.1016/j.geomorph.2019.04.029

Pétursson HG, Norðdahl H, Ingólfsson Ó (2015) Late Weichselian history of relative sea level changes in Iceland during a collapse and subsequent retreat of marine based ice sheet. Cuad Investig Geográfica 41:261. https://doi.org/10.18172/cig.2741
Phillips M, Wolter A, Lüthi R, Amann F, Kenner R, Bühler Y (2017) Rock slope failure in a recently deglaciated permafrost rock wall at Piz Kesch (Eastern Swiss Alps), February 2014. Earth Surf Process Landforms 42:426–438. https://doi.org/10.1002/esp.3992
Pudasaini SP (2012) A general two-phase debris flow model. J Geophys Res Earth Surf 117:1–28. https://doi.org/10.1029/2011JF002186
Pudasaini SP, Krautblatter M (2014) Journal of Geophysical Research : Earth Surface A two-phase mechanical model for rock-ice avalanches. 2272–2290. 10.1002/2014JF003183.Received
Ravanel L, Magnin F, Deline P (2017) Impacts of the 2003 and 2015 summer heatwaves on permafrost-affected rock-walls in the Mont Blanc massif. Sci Total Environ 609:132–143. https://doi.org/10.1016/j.scitotenv.2017.07.055
Remondino F, Spera MG, Nocerino E, Menna F, Nex F (2014) State of the art in high density image matching. Photogramm Rec 29:144–166. https://doi.org/10.1111/phor.12063
Rickenmann D (1999) Empirical relationships for debris flows. Nat Hazards 19:47–77. https://doi.org/10.1023/A:1008064220727
Roberti G, Friele P, de Vries B v W et al (2017) Rheological evolution of the Mount Meager 2010 debris avalanche, southwestern British Columbia. Geosphere 13:369–390
Sæmundsson Þ, Morino C, Helgason JK, Conway SJ, Pétursson HG (2018) The triggering factors of the Móafellshyrna debris slide in northern Iceland: Intense precipitation, earthquake activity and thawing of mountain permafrost. Sci Total Environ 621:1163–1175. https://doi.org/10.1016/j.scitotenv.2017.10.111
Scheidegger AE (1973) On the prediction of the reach and velocity of catastrophic landslides. Rock Mech Rock Eng 5:231–236
Schneider D, Huggel C, Haeberli W, Kaitna R (2011a) Unraveling driving factors for large rock-ice avalanche mobility. Earth Surf Process Landforms 36:1948–1966. https://doi.org/10.1002/esp.2218
Schneider D, Kaitna R, Dietrich WE, Hsu L, Huggel C, McArdell BW (2011b) Frictional behavior of granular gravel-ice mixtures in vertically rotating drum experiments and implications for rock-ice avalanches. Cold Reg Sci Technol 69:70–90. https://doi.org/10.1016/j.coldregions.2011.07.001
Schwab JW, Geertsema M, Evans SG (2003) Catastrophic rock avalanches, west-central BC, Canada. In: 3rd Canadian Conference on Geotechnique and Natural Hazards. Edmonton, AB, pp 52–259
Sheridan P, Smith S, Brown A, Vosper S (2010) A simple height-based correction for temperature downscaling in complex terrain. Meteorol Appl 17(3):329–339
Shreve RL (1968) The Blackhawk Landslide. The Geological Society of America, Inc., Boulder, Colorado
Sigfússon A, Thoroddsen Á, Aðalsteinsdóttir ÁK et al (2016) Hvalárvirkjun í Ófeigsfirði Matsskýrsla. Reykjavík, Iceland
Smith MW, Carrivick JL, Quincey DJ (2015) Structure from motion photogrammetry in physical geography. Prog Phys Geogr 40:247–275. https://doi.org/10.1177/0309133315615805
Snavely N, Seitz SM, Szeliski R (2008) Modeling the world from Internet photo collections. Int J Comput Vis 80:189–210. https://doi.org/10.1007/s11263-007-0107-3
Sosio R (2015) Rock-Snow-Ice Avalanches. In: Davies T (ed) Landslide Hazards, Risks, and Disasters. p 191'240
Sosio R, Crosta GB, Chen JH, Hungr O (2012) Modelling rock avalanche propagation onto glaciers. Quat Sci Rev 47:23–40. https://doi.org/10.1016/j.quascirev.2012.05.010
Tost M, Cronin SJ, Procter JN (2014) Transport and emplacement mechanisms of channelised long-runout debris avalanches, Ruapehu volcano, New Zealand. Bull Volcanol 76:1–14. https://doi.org/10.1007/s00445-014-0881-z
Tussetschläger H, Brynjólfsson S, Brynjólfsson S et al (2020) Perennial snow patch detection based on remote sensing data on Tröllaskagi Peninsula, northern Iceland. JOKULL 69:103–128. https://doi.org/10.33799/jokull2019.69.103
Tveito OE, Førland E, Heino R, et al (2000) Nordic temperature maps. Oslo, Report 4 09/00
Vallance JW, Scott KM (1997) The Osceola Mudflow from Mount Rainier: sedimentology and hazard implications of a huge clay-rich debris flow. Bull Geol Soc Am 109:143–163. https://doi.org/10.1130/0016-7606(1997)109<0143:TOMFMR>2.3.CO;2
Varnes DJ (1978) Slope movement types and processes. Transp Res Board Spec Rep 11–33. In Special report 176: Landslides: Analysis and Control, Transportation Research Board, Washington, D.C.
Voight B, Sousa J (1994) Lessons from Ontake-san: a comparative analysis of debris avalanche dynamics. Eng Geol 38:261–297. https://doi.org/10.1016/0013-7952(94)90042-6
Walter F, Amann F, Kos A, Kenner R, Phillips M, de Preux A, Huss M, Tognacca C, Clinton J, Diehl T, Bonanomi Y (2020) Direct observations of a three million cubic meter rock-slope collapse with almost immediate initiation of ensuing debris flows. Geomorphology 351:106933
Westoby MJ, Brasington J, Glasser NF, Hambrey MJ, Reynolds JM (2012) "Structure-from-Motion" photogrammetry: a low-cost, effective tool for geoscience applications. Geomorphology 179:300–314. https://doi.org/10.1016/j.geomorph.2012.08.021
Xu Q, Shang Y, van Asch T, Wang S, Zhang Z, Dong X (2012) Observations from the large, rapid Yigong rock slide – debris avalanche, southeast Tibet. Can Geotech J 49:589–606. https://doi.org/10.1139/t2012-021

C. Morino
Laboratoire EDYTEM,
Université Savoie Mont Blanc, UMR-CNRS 5204,
Chambéry, France

C. Morino · T. Argles
School of Environment, Earth & Ecosystem Sciences,
The Open University,
Milton Keynes, UK

C. Morino (✉) · S. J. Conway
Laboratoire de Planétologie et Géodynamique,
Université de Nantes UMR-CNRS 6112,
Nantes, France
Email: costanza.morino@gmail.com

M. R. Balme
School of Physical Sciences,
The Open University,
Milton Keynes, Walton Hall, UK

J. K. Helgason
Icelandic Meteorological Office,
Avalanche Research Centre,
Ísafjörður, Iceland

Þ. Sæmundsson
Department of Geography and Tourism,
University of Iceland,
Reykjavík, Iceland

C. Jordan
British Geological Survey,
Environmental Science Centre,
Keyworth, UK

J. Hillier
Geography and Environment,
Loughborough University,
Loughborough, UK